



## King's Research Portal

DOI:

[10.1126/scitranslmed.aaw2064](https://doi.org/10.1126/scitranslmed.aaw2064)

*Document Version*

Peer reviewed version

[Link to publication record in King's Research Portal](#)

*Citation for published version (APA):*

Hutson, T. H., Kathe, C., Palmisano, I., Bartholdi, K., Hervera, A., De Virgiliis, F., McLachlan, E., Zhou, L., Kong, G., Barraud, Q., Danzi, M. C., Medrano-Fernandez, A., Lopez-Atalaya, J. P., Boutillier, A. L., Sinha, S. H., Singh, A. K., Chaturbedy, P., Moon, L. D. F., Kundu, T. K., ... Di Giovanni, S. (2019). Cbp-dependent histone acetylation mediates axon regeneration induced by environmental enrichment in rodent spinal cord injury models. *Science Translational Medicine*, 11(487), [eaaw2064]. <https://doi.org/10.1126/scitranslmed.aaw2064>

### **Citing this paper**

Please note that where the full-text provided on King's Research Portal is the Author Accepted Manuscript or Post-Print version this may differ from the final Published version. If citing, it is advised that you check and use the publisher's definitive version for pagination, volume/issue, and date of publication details. And where the final published version is provided on the Research Portal, if citing you are again advised to check the publisher's website for any subsequent corrections.

### **General rights**

Copyright and moral rights for the publications made accessible in the Research Portal are retained by the authors and/or other copyright owners and it is a condition of accessing publications that users recognize and abide by the legal requirements associated with these rights.

- Users may download and print one copy of any publication from the Research Portal for the purpose of private study or research.
- You may not further distribute the material or use it for any profit-making activity or commercial gain
- You may freely distribute the URL identifying the publication in the Research Portal

### **Take down policy**

If you believe that this document breaches copyright please contact [librarypure@kcl.ac.uk](mailto:librarypure@kcl.ac.uk) providing details, and we will remove access to the work immediately and investigate your claim.

# Environmental enrichment induces axon regeneration and recovery after peripheral and spinal injuries via activity mediated CBP-dependent histone acetylation: a druggable pathway

T. H. Hutson<sup>1</sup>, C. Kathe<sup>2,3</sup>, I. Palmisano<sup>1</sup>, K. Bartholdi<sup>3</sup>, A. Hervera<sup>1</sup>, F. De Virgiliis<sup>1</sup>, E. McLachlan<sup>1</sup>, L. Zhou<sup>1,4</sup>, G. Kong<sup>1,4</sup>, Q. Barraud<sup>3</sup>, M. C. Danzi<sup>5</sup>, A. Medrano-Fernandez<sup>6</sup>, J. Lopez-Atalaya<sup>6</sup>, A. L. Boutillier<sup>7</sup>, S. H. Sinha<sup>8</sup>, A. K. Singh<sup>8</sup>, P. Chaturbedy<sup>9</sup>, L. D. F. Moon<sup>2</sup>, T. K. Kundu<sup>8</sup>, J. L. Bixby<sup>5</sup>, V. P. Lemmon<sup>5</sup>, A. Barco<sup>6</sup>, G. Courtine<sup>3,#</sup>, and S. Di Giovanni<sup>1,4,#,\*</sup>

1. Centre for Restorative Neuroscience, Division of Brain Sciences, Department of Medicine, Imperial College London, London, UK.

2. Neurorestoration Group, Wolfson Centre for Age-Related Diseases, King's College London, London, UK.

3. Brain Mind Institute and Center for Neuroprosthetics, Ecole Polytechnique Fédérale de Lausanne (EPFL), Geneva, Switzerland.

4. Hertie Institute for Clinical Brain Research, University of Tübingen, Tübingen, Germany.

5. The Miami Project to Cure Paralysis, University of Miami, Miami, FL, USA.

6. Instituto de Neurociencias, Universidad Miguel Hernandez Consejo Superior de Investigaciones Científicas, Alicante, Spain.

7. Université de Strasbourg, CNRS, UMR 7364, Laboratoire de Neurosciences Cognitives et Adaptatives (LNCA), F-67000 Strasbourg, France.

8. Transcription and Disease Laboratory, Jawaharlal Nehru Centre for Advanced Scientific Research, Bangalore, India.

9. Nanomaterials and Catalysis Laboratory, Chemistry and Physics of Materials Unit, JNCASR, Bangalore, India.

# Co-senior authors

\*Correspondence: s.di-giovanni@imperial.ac.uk

**One Sentence Summary:** Environmental enrichment or pharmacological mediated CBP-dependent histone acetylation increases regeneration potential of specific classes of neurons.

**Abstract:** Injured axons fail to regenerate in the adult mammalian central nervous system (CNS), leading to permanent deficits in sensory and motor functions. We found that enhancing the activity of proprioceptive dorsal root ganglion (DRG) neurons through an enriched environment induces a long-lasting increase in their regenerative potential that is dependent on CREB Binding Protein (CBP)-mediated histone acetylation. Delivery of a small molecule activator of CBP acetyltransferase at clinically relevant times after spinal cord injury promoted regeneration and sprouting of sensory and motor axons, together with improvement in both sensory and motor functions. These findings open avenues for therapeutic developments in clinical spinal cord injury.

## Introduction

Following spinal cord injury (SCI), motor and sensory axons fail to regenerate, leading to permanent neurological impairments (1, 2). This absence of CNS regeneration after injury has been attributed to two main interconnected factors: the presence of growth inhibitory molecules in the CNS and the lack of an effective neuronal-intrinsic regenerative response (2-4). While axon regeneration fails in the CNS after injury, limited regeneration and partial functional recovery do occur in the injured peripheral nervous system (PNS) (5, 6). The best-established method for increasing the intrinsic regenerative capacity of sensory neurons in the dorsal root ganglion (DRG) consists of inducing a conditioning injury to the axons in the sciatic nerve prior to the CNS injury (7-9). While this has provided useful insights in the mechanisms underlying axon regeneration, a conditioning lesion only induces modest regeneration in the CNS and is not a clinically viable approach.

Sensory dorsal root ganglia (DRG) neurons convey afferent information from the periphery to the spinal cord in order to modulate motor outputs, and to supraspinal structures for the elaboration of sensorimotor integration and conscious perception. Amongst the DRG, proprioceptive neurons innervate muscle spindles and Golgi tendon organs. They transmit information about the length and tension of muscles, which plays a critical role during sensorimotor execution (10, 11). Moreover, proprioceptive afferent feedback plays an important role in directing motor recovery after SCI. Mice lacking functional proprioceptive afferents exhibit a defective rearrangement of descending pathways that prevents recovery after SCI (11). This observation indicates that proprioceptive neurons may deliver molecular cues for axonal regrowth and sprouting after injury. In turn, modulation of proprioceptive afferents with electrical stimulation (12, 13) and rehabilitative training (14) augments neuroplasticity and recovery in both animal models and humans after SCI (15). However, the underlying mechanisms remain poorly understood.

Proprioceptors are ideally located for modulation by environmental stimuli. Here, we investigated the impact of environmental enrichment (EE) on proprioceptive DRG neurons, hypothesizing that this would prime them to initiate a regenerative response to a subsequent injury, similar to a conditioning injury. We show that augmenting the activity of proprioceptive DRG neurons using EE induces a lasting increase in their regenerative potential that is dependent on CREB Binding Protein (CBP)-mediated histone acetylation. In turn, pharmacologically increasing CBP acetyltransferase activity at clinically-relevant times and in clinically-relevant models of SCI promoted regeneration and sprouting of sensory axons and brainstem motor pathways that mediated improvements in both sensory and motor functions. These results show that neuronal activity leads to changes in chromatin environment that boost the regenerative capacity of neurons. Elucidating the mechanisms underlying activity-dependent responses in neurons translated into the identification of a clinically-relevant pharmacotherapy for SCI that warrants evaluation in humans.

## Results

### **Environmental enrichment induces a lasting increase in the regenerative potential of DRG neurons**

To test whether EE can enhance the regenerative potential of DRG neurons, mice were exposed to EE or standard housing (SH) for 1, 3, 6, 10 or 35 days. Neurite outgrowth of DRG neurons was significantly enhanced only after exposure to EE for 10 or 35 days on a growth permissive substrate (Fig. 1A and B). The extent of neurite outgrowth on myelin was similar to what is observed after a conditioning injury (Fig. S1), which represents the benchmark for stimulating DRG axon regeneration (9, 16).

EE-dependent neurite outgrowth was abolished when delivering the transcriptional inhibitor actinomycin-D in culture (Fig. S2), suggesting a dependence of this response on gene transcription. EE-dependent increase in neurite outgrowth was maintained during a 5-week period of SH after 10 days of EE (Fig. 1C, D and E), suggesting that EE may trigger long-

lasting epigenetic reprogramming. Analyses of growth responses revealed that EE enhanced axon elongation rather than branching (Fig. S3), which may translate into axonal regeneration *in vivo*.

Given the multifactorial nature of EE, we decided to discriminate between the relative role of running, which has previously been shown to enhance peripheral nerve regeneration (17) and the remaining environmental stimuli (larger cage, increased number of mice, novel objects, and increased nesting material) on DRG outgrowth. Mice were placed either in EE, in SH, in EE with an immobilised wheel or in SH with a running wheel for 10 days. Analysis of neurite outgrowth showed that although the running wheel in SH enhanced outgrowth compared to SH alone, the full complement of EE still induced a significantly higher degree of outgrowth (Fig. S4). This result indicated that the full EE is required for maximal enhancement of DRG outgrowth.

We next tested whether EE can also enhance regeneration of axons within the peripheral and the central nervous system. Prior exposure to EE enhanced sciatic nerve regeneration after complete transection and reanastomosis (Fig. 1F and G), along with increased muscle reinnervation after a sciatic nerve crush (Fig. S5).

We then assessed whether pre-exposure to EE would enhance regeneration of sensory axons in the dorsal columns after a SCI and compared this response to the regeneration observed after a conditioning injury. Three groups of adult mice were exposed to EE or SH for 10 days and then housed in SH, subsequently one SH group received a conditioning sciatic nerve axotomy (SNA) injury and the other SH and the EE groups underwent a sham injury. Next, all the mice received a thoracic (T12) dorsal hemisection. Five weeks later, the retrograde tracer Cholera Toxin subunit B (CTB) was injected into the sciatic nerves to evaluate the regeneration of ascending dorsal column axons (Figure 1H). The majority of labelled axons from SH Sham mice retracted from the injury site. In contrast, labelled axons from EE Sham mice could be observed within the lesion epicentre. Some regenerating axons even expanded beyond the lesion site, attaining distance up to 800  $\mu$ m from the lesion border (Figure 1H and I). Some of these regenerating axons co-localized with vGlut1, suggesting the formation of putative synapses (Fig. S6). In the SH SNA group, we also found as expected axons traversing the lesion epicenter (Figure 1H and I).

We conducted terminal electrophysiological experiments 6 weeks after injury to evaluate the functionality of these regenerating axons. The dorsal columns were stimulated below the injury at L5, and recorded both below and above the lesion, at L1 and T9, respectively (Figure 1J). In all the animals that underwent EE or SNA, compound action potentials could be recorded above the lesion site. However, the amplitude of these responses was significantly larger for the animals that had been housed in EE compared to SNA (black traces, Figure 1K and L), suggesting an increase in neuroplasticity across the lesion. There was no significant difference in the compound action potential recordings below the lesion for any of the groups (blue traces, Figure 1K).

To assert that regenerating sensory axons were responsible for the increase in conduction through the lesion site, we specifically silenced these axons using designer receptors exclusively activated by designer drugs (DREADD), using methods that were described previously (18). We injected an AAV-flex-hM4Di into the sciatic nerve to express the Gi receptor into DRG neurons under Cre recombination. Three weeks after SCI, an AAV-Cre was injected rostral to the site at of injury to express the Cre-dependent Gi-coupled DREADD only in those DRG neurons that had extended axons through and beyond the lesion. After 3 additional weeks, mice previously exposed to EE underwent electrophysiological assessment. In all tested mice, compound action potentials could be recorded beyond the lesion. Chemogenetic mediated silencing restricted to regenerated axons (Cre-dependent AAV-flex-hM4Di) significantly reduced conduction across the lesion, establishing causality that was confirmed with a re-transection (Fig. 1K and L).



### **Proprioceptive afferent feedback is required for EE-mediated increase in DRG regenerative growth**

We next investigated whether a specific type of neurons were implicated in EE-dependent regenerative growth. We injected CTB into the distal sciatic nerve one day after performing a sciatic nerve crush injury. Consequently, only DRG neurons that regenerated an axon across the injury site and into the denervated side would be able to take up the CTB tracer (Figure 2A). Two days after the CTB injection, we assessed the number of CTB-positive DRG neurons that co-stained for markers of the main DRG subpopulations (Figure 2B). Prior exposure to EE significantly increased the number of CTB positive DRG neurons (Figure 2C). The majority of DRG neurons, which regenerated axons through the sciatic nerve crush and were retrogradely labeled with CTB, expressed markers of proprioceptors (parvalbumin) rather than nociceptors (isolectin B4 or substance P) (Figure 2B and D), suggesting that EE specifically enhances the regeneration of proprioceptive axons.

Next, we investigated whether the EE-dependent increase in regenerative potential of proprioceptive neurons relied on a muscle spindle proprioceptive mechanism. To this end, we used *Egr3*<sup>-/-</sup> mice that while retaining a similar number of parvalbumin (PV) DRG neurons compared to WT mice, this mutation abolishes muscle spindle proprioceptive feedback (11, 19) (Figure 2E). We found that EE- but not conditioning injury-dependent DRG outgrowth was abolished in mice lacking intact muscle spindles (*Egr3*<sup>-/-</sup>) (Figure 2F and G). This observation demonstrates that EE-dependent regenerative priming is contingent on intact proprioceptive feedback.

Finally, to further confirm the cell type specificity of the EE mechanism, we assessed neurite outgrowth of DRG neurons from mice that expressed tdTomato under the control of the PV promoter. Exposure to EE significantly increased the outgrowth of tdTomato positive (PV<sup>ON</sup>) but not tdTomato negative (PV<sup>OFF</sup>) DRG neurons (Figure 2H and I).

Taken together, these experiments demonstrate that prior exposure to EE specifically primes proprioceptive DRG neurons for enhanced axon regeneration.

### **Environmental enrichment induces signaling pathways involved in neuronal activity, calcium mobilization and the regenerative program of large-diameter DRG neurons**

EE and exercise have been shown to increase neurotrophin expression and modify cytokines influencing neuroplasticity (17, 20-22). Surprisingly we found no changes in neurotrophin or cytokines levels in the DRG or in the blood (Fig. S7), suggesting that alternative mechanisms may be responsible for EE-dependent DRG regenerative growth.

To uncover EE-dependent molecular mechanisms, we performed RNA sequencing (RNAseq) from whole DRG or laser-captured large-diameter DRG neurons (LDN) and conducted proteomic analysis from sciatic nerve axoplasm after EE or SH. Unsupervised gene expression clustering showed dramatic changes in gene expression of LDN after EE vs SH, but not in the whole DRG, which contains a multitude of different neuronal and glial cell types (Figure 3A, Fig. S8A, Files S1 and S2). These results confirmed that EE specifically modulates gene expression in proprioceptors and potentially mechanoreceptors. EE preferentially increased rather than repressed gene expression in LDN (Fig. S8B). Similarly, proteomic analysis showed a larger number of up-regulated proteins after EE vs SH (71 vs 49, Fig. S8C and File S3). Importantly, 37 out of 71 significantly up-regulated proteins were also up-regulated at the RNA level, suggesting that gene transcription drove more than half of the observed protein changes (File S4). Functional classification of EE-dependent gene expression changes in LDNs revealed that EE strongly modulated functionally interconnected molecular pathways involving ion channels, neuronal activity, calcium signaling, energy metabolism and neuronal projection (Figure 3B, Fig. S8D and E, Files S5, S6, S7). Combined analysis of the RNAseq and proteomic datasets for protein-protein interactions identified multiple interactions between proteins involved in neuronal activity, calcium signaling and cytoskeletal rearrangements, supporting a role for EE-mediated activity in axon projection and elongation.

These results encouraged us to investigate the role of neuronal activity and calcium release in the EE-mediated increase in DRG regenerative potential. We employed an AAV-mediated chemogenetics approach to inhibit or enhance neuronal activity of DRG neurons using DREADD technology. When activated by the pharmacologically inert ligand clozapine-N-oxide (CNO), Gi-coupled (hM4Di) DREADD receptors inhibit adenylyl cyclase, which silences neuronal activity (23). Instead, activation of Gq-coupled (hM3Dq) DREADD receptors enhance neuronal activity by eliciting IP<sub>3</sub>-mediated calcium release from intracellular stores (23). This increase in intracellular calcium levels activates calcium-dependent signalling cascades, which would thus mimic the effects of EE on DRG neurons identified with gene and proteomic analysis.

We injected AAV vectors into the sciatic nerve to express hM4Di, hM3Dq or GFP in DRG neurons. mCitrine/GFP expression confirmed an efficient transduction (Fig. S9). Four weeks after injection, mice expressing hM4Di, hM3Dq or GFP were placed in EE or SH. CNO was added in the drinking water to activate the receptors. Ten days later, we performed a sciatic nerve crush, and assessed the extent of regeneration three days post-injury (Figure 3C and D).

Gq activation enhanced axon regeneration in SH mice and Gi-dependent inactivation of DRG neurons significantly attenuated axon regeneration of mice exposed to EE, demonstrating the importance of neuronal activity for EE-mediated regeneration (Figure 3C and D). Expression of Gi in SH mice or Gq in EE mice did not further impair or promote axon regeneration (Figure 3C and D). Similar results were obtained when assessing neurite outgrowth of DRGs cultured after *in vivo* DREADD transduction and EE exposure (Fig. S10). Gq expression in DRGs from SH mice significantly increased neurite outgrowth to a similar extent to what was observed in the DRGs of mice exposed to EE, while the expression of Gi in DRG neurons significantly reduced EE-dependent outgrowth (Fig. S10).

RNAseq and proteomics data suggests that EE may enhance calcium signalling in proprioceptive DRG neurons. To visualize this induction of activity-dependent signaling pathways in proprioceptive neurons in response to EE, we directly measured intracellular calcium levels in these cells, as an indicator of release from intracellular stores. Transgenic mice that expressed the genetically encoded calcium indicator GCaMP under the PV promoter were exposed to EE or SH. Whole sciatic DRGs were extracted in order to measure the fluorescent signals of proprioceptive neurons *ex vivo* when applying increasing levels of potassium chloride. As anticipated, we found that a prior exposure to EE significantly increased the levels of calcium in DRG neurons at all the potassium chloride concentrations tested compared to calcium levels measured in the DRGs of SH mice (Figure 3E and F, time-lapse videos S1 and S2). These observations show that EE increases calcium signalling in proprioceptive neurons, which is likely due to the increased solicitation of muscle spindles and force sensors within the enriched environment.

These results provide evidence that EE increases neuronal activity and calcium signalling in proprioceptive DRG neurons and plays an important role in the activity-dependent increase in regenerative potential.

### **CBP mediated histone acetylation is required for EE-dependent increase in regeneration potential**

We reasoned that EE-dependent modulation of neuronal activity might induce epigenetic modifications enabling active transcription and a lasting increase in regenerative potential. Indeed, we found that EE enhanced H3K27ac and H4K8ac but not H3K9ac, H3K4me2 or H3K4me3 in parvalbumin-positive DRG neurons (Figure 4A, B and E, Fig. S11). H4K8ac and H3K27ac are both well-established markers of transcriptional activation, which correlated with our RNAseq data where we observed activation of gene expression in the large-diameter sensory neurons after EE (Fig. S8B). These two histones can be acetylated by CREB-binding protein (CBP) (24, 25), a lysine acetyltransferase that contains two calcium-sensitive transactivation domains (26) and involved in activity-dependent neuroplasticity (27-29).

Acetylation of CBP increases its acetyltransferase activity and facilitates transcription complex formation and acetylation of H4K8 and H3K27, leading to persistent changes in transcriptional activity (30, 31). EE significantly increased pCREB (Figure 4C, D and F) and active acetylated-CBP (acCBP) expression in parvalbumin-positive DRG neurons (Figure 4G and H). Levels of H4K8ac but not pCREB or acCBP remained elevated in PV<sup>ON</sup> DRG neurons 5 weeks after exposure to EE (Fig. S12). The levels of histone acetylation are likely maintained because they do not rely solely upon the histone deacetylase/acetyltransferase equilibrium but on the overall epigenetic configuration of the locus. While this is important for histones, it is unlikely for proteins, such as CBP, whose acetylation status directly depends on the activity of signal transduction pathways. Furthermore, the levels of H4K8ac and acCBP in DRG neurons were enhanced or inhibited by hM3Dq or hM4Di, respectively (Fig. S13), linking calcium-dependent neuronal activity to histone acetylation.

To further elucidate the role of CBP in the EE-mediated increase in the regenerative potential of DRG neurons, we used CaMKIIa-creERT2/CBP<sup>f/f</sup> transgenic mice with tamoxifen inducible CBP deletion in CaMKIIa positive cells (29). This population of neurons includes both large and medium diameter DRG neurons (32) (Figure S14). Four weeks after tamoxifen treatment, mice were placed in EE or SH for five weeks prior to the extraction of the sciatic DRG neurons. Neurite outgrowth was then assessed in culture. Importantly, the conditional deletion of CBP in CaMKIIa-positive DRG neurons (29) abolished the EE-dependent increase in neurite outgrowth (Figure 4I and J). This data suggests that CBP specifically contributes to mediating the increase in regenerative potential of DRG neurons after EE exposure. We also found that CBP deletion completely abolished the EE-mediated increase in H4K8ac (Figure 4K), ruling out a significant role for other histone acetyltransferases.

### **Pharmacological activation of CBP/p300 promotes sensory axon regeneration and recovery after a dorsal hemisection SCI in mice**

The central role of CBP suggested that the pharmacological activation of CBP might mimic the EE-dependent increase in regenerative growth of DRG neurons. To test this hypothesis, we delivered a small-molecule activator of CBP/p300 (TTK21) after SCI. A recent study has shown that TTK21 is non-toxic, and when conjugated to glucose derived carbon nanospheres (CSP), TTK21 successfully crosses the blood brain barrier, effectively enhances histone acetylation in the hippocampus, and promotes improvements in learning and memory capacities (33).

We first confirmed that the addition of CSP-TTK21 to DRG cultures was capable of increasing neurite outgrowth compared to control CSP. Indeed, CSP-TTK21, a pharmacological activator of CBP/p300 (33), triggered a significant increase in neurite outgrowth and H4K8ac in cultured neurons (Figure 5A and B). We next tested whether CSP-TTK21 could promote axonal regeneration *in vivo* following a mid-thoracic dorsal hemisection (Figure 5C). Injured mice received a weekly i.p. injection of 20 mg/kg CSP-TTK21 or control CSP, beginning 4 hours after injury. To assess regeneration of sensory axons in the dorsal columns, we injected the sciatic nerves with CTB tracer and examined the spinal cord six weeks after SCI (Figure 5D). Treatment with CSP-TTK21 promoted sensory axon regeneration up to 1000  $\mu$ m rostral to the lesion (Figure 5E and F). We conducted behavioural assessments for five weeks after SCI to evaluate recovery of sensorimotor function. We selected tasks contingent on accurate proprioceptive information, which included the Gridwalk and adhesive tape test. We observed a decrease in the number of hindlimb slips in the gridwalk test (Figure 5G) and a superior recovery in the time it took to sense and then remove a piece of adhesive tape placed on the hindpaws after treatment with CSP-TTK21 (Figure 5H, Fig. S15). Many of the regenerating axons from the CSP-TTK21 treated mice co-localized with vGlut1, suggesting the formation of putative synapses (Figure 5I and J). We then assessed the functionality of these regenerating axons with terminal electrophysiological experiments. We found a significant increase in the amplitude of compound action potentials recorded above the SCI in

treated mice compared to the control group, demonstrating that the CBP activator increased neural conduction across the lesion site (Figure 5K and L). In addition to promoting axon regeneration across the lesion site, we investigated whether CSP-TTK21 also increased sprouting of axons below the level of injury. CSP-TTK21 enhanced the number of vGlut1-positive boutons apposed to motoneurons (putative synapses) in the ventral horn of the lumbar enlargement (Figure 5M and N), suggesting spinal circuit reorganization and sprouting of group-Ia proprioceptive afferents below the injury. This reorganization of proprioceptive afferents has previously been associated with functional recovery (11, 14). We also observed a significant increase in the intensity of vGlut1 staining in lamina V of the spinal cord after CSP-TTK21 treatment (Fig. S16). Importantly, CSP-TTK21 treatment significantly increased H4K8ac within DRG neurons (Fig. S17), but did not affect the scar area or GFAP intensity (Fig. S18).

### **Pharmacological CBP/p300 activation enhances sprouting of both descending motor and ascending sensory axons leading to functional recovery after contusion SCI in rats**

To further substantiate the efficacy of CSP-TTK21 *in vivo*, we evaluated whether CSP-TTK21 could promote anatomical and functional neuroplasticity of motor systems after a more clinically relevant SCI. Adult rats underwent a mid-thoracic spinal cord contusion (220 kdyn). CSP-TTK21 or CSP was administered *i.p.* 6 hours after SCI, which is a clinically-relevant time point after injury, and repeated weekly thereafter.

To quantify locomotor performance, we applied a principal component (PC) analysis to various parameters calculated from kinematic recordings of quadrupedal walking along a flat corridor. PC1 captured the extent of the recovery, showing that CSP-TTK21 significantly improved locomotor performance compared to CSP-treated rats. Parameters that correlated with improved recovery included reduced paw dragging, increased step height and more frequent plantar steps with weight bearing (Figure 6A-D, Video S3). The number of footfalls occurring during locomotion across a horizontal ladder also decreased significantly (Fig. S19). This functional recovery was associated with increased sprouting of descending reticulospinal and serotonergic axons within the lumbar spinal cord (Figure 6E-J). Accordingly, CSP-TTK21 enhanced H4K8ac in the reticular formation and raphe nucleus (Fig. S20). CSP-TTK21 also augmented the density of vGlut1-positive boutons from proprioceptors onto motoneurons located within lumbar segments below the injury (Figure 6K and L), which was associated with increased muscle responses evoked by stimulating proprioceptive afferents (H-reflex, Figure 6M). However, CSP-TTK21 did not affect the lesion size or GFAP intensity (Fig. S21).

Together, these results show that activating CBP using a small-molecule promotes sprouting of descending pathways and proprioceptive afferents below injury associated with improved recovery of both sensory and motor functions after SCI.

### **Discussion**

Our work demonstrates how increasing the neuronal activity of proprioceptive DRG neurons prior to an injury using EE or chemogenetics elicits CBP-mediated histone acetylation that is required for the enduring increase in axonal regeneration potential. Activating CBP using a small-molecule at clinically relevant time points and in clinically-relevant models of SCI mimicked the effect of increasing neuronal activity. CSP-TTK21 treatment promoted regeneration of ascending sensory axons and sprouting of both sensory and supraspinal motor axons below the lesion. The induced spinal circuit reorganization resulted in significant electrophysiological and behavioral recovery. Here, we discuss the role of activity on enhancing the regeneration potential of proprioceptive neurons as well as the molecular mechanisms underlying these effects before concluding on the implications for spinal cord repair and rehabilitation.

### **Activity-dependent mechanisms for priming the regeneration potential of proprioceptive neurons**

The complete lack of EE-mediated increase in neurite outgrowth observed in DRGs from mice with defective muscle spindle receptors demonstrates the importance of proprioceptive neurons and muscle spindle afferent feedback in triggering the activity-dependent increase in regeneration potential. This finding provides novel evidence and expands upon the recent demonstration that muscle spindle feedback is essential for inducing the correct anatomical reorganisation of projection neurons and functional recovery after spinal cord injury (11). Multiple pieces of evidence emphasised this remarkable cell type specificity. Furthermore, we found that EE drives the expression of genes underlying neuronal activity, calcium signalling and regenerative pathways in large-diameter DRG neurons. Indeed, this robust gene expression response was largely lost when RNAseq was performed from the whole DRG that contains multiple neuronal populations and glial cells, highlighting the specificity of EE-mediated gene-expression in large-diameter DRG neurons, which are essentially composed of cells innervating proprioceptors. Finally, the impact of neuronal activity on axon regeneration could be reproduced experimentally. We showed that the manipulation of DRG neuronal activity using chemogenetics reproduced or abolished EE-mediated increase in axonal regeneration potential. Indeed, the increase in DRG neuronal activity alone triggered an increase in axon regeneration, further expanding upon what has been observed recently (34, 35).

These data suggest that the effects of EE are essentially elicited by proprioceptive feedback signals, which leads to an enhanced activity of proprioceptive DRG neurons that promotes a lasting augmentation of their regenerative potential.

### **Lasting increase in regeneration potential involves CBP-dependent histone acetylation**

Our results provided evidence that the lasting increase in regeneration potential resulted from a CBP-dependent increase in histone acetylation and a dramatic increase in gene expression, including pathways involved in neuronal activity, axonal projection and cytoskeleton remodelling. Specifically, neuronal activity elicited by EE activates CBP and increases the acetylation of H4K8. This enduring increase in histone acetylation likely mediates the long-lasting enhancement in regenerative potential of these DRG neurons that extends for several weeks. The requirement of CBP was confirmed as deletion of CBP completely abrogated the EE-dependent increase in DRG neurite outgrowth and H4K8 acetylation. Furthermore, pharmacological activation of CBP after SCI promoted axonal regeneration and functional recovery. These data show that CBP is necessary for the EE-mediated increase in DRG neurite outgrowth and that its activation promotes functionally relevant axon regeneration and sprouting leading to recovery. These results expand upon recent studies by us and others showing that associated histone acetylation with a transcriptional-dependent enhancement of the regeneration program in neurons (36-41). We previously demonstrated that a conditioning injury activates p300/CBP associated factor (PCAF). Together with HAT p300, PCAF promotes acetylation of the promoters of known regeneration associated genes (RAGs), which facilitate their expression and thereby enhance axon regeneration after injury (36, 38, 39). The inhibition of HDACs promotes histone acetylation that can also promote axon regeneration (37, 40). Similarly, nuclear export of HDAC5 has been shown to be required for peripheral axon regeneration and for the induction of a number of RAGs (41). However, our present results show that EE-dependent histone acetylation does not involve PCAF since H3K9ac is not altered by EE and it does not require p300, since CBP deletion completely blocked EE-dependent DRG regenerative growth. These observations suggest that a conditioning injury and EE operate via separate signalling mechanisms leading to distinct histone acetylation changes. However, a limitation of the present and previous studies is the lack of systematic screening for post-translational histone modifications that affect the histone code and gene transcription. The systematic measurement of histone acetylation and methylation could lead



to the identification of additional histone modifying enzymes that modulate EE-dependent or conditioning-dependent axonal regeneration in addition to CBP/p300 and PCAF.

Collectively, these studies demonstrate the importance of the chromatin environment for the regenerative capacity of DRG neurons. Identifying and manipulating key histone modifiers that can orchestrate broad changes in gene transcription may lead to significant improvements in axon regeneration.

### **Implications for spinal cord repair and rehabilitation**

The identification of the mechanisms underlying the activity-dependent increase in DRG regenerative growth allowed us to reproduce these effects pharmacologically. We show that the activation of CBP within a clinically relevant time frame after SCI using a non-toxic small molecule promotes regeneration of ascending and descending axons. CBP activation also triggered a robust sprouting of proprioceptive fibers below the injury, within the lumbar motor circuitry. These changes correlated with enhanced electrophysiological and behavioural functional recovery in sensory and motor tests. Although the specific contribution from each reorganized system remains unclear, we surmise that the reorganization of proprioceptive feedback circuits below the injury is more important to improve precision walking than the relatively short-distance regeneration of ascending fibers. While the specific mechanisms of recovery require to be studied further, these combined findings show that activity-dependent regenerative pathways triggered preceding a SCI can also be successfully targeted to enhance axon sprouting, regeneration and sensorimotor recovery after injury.

Rehabilitation strategies including exercises that increase afferent activity in the spinal cord are now well established to augment functional recovery in rodents after SCI, although their effect on axon regeneration in the CNS is not clear (42-44). Moreover, modulation of proprioceptive afferent circuits with electrical stimulation augments neuroplasticity and recovery after a SCI (13, 14, 45, 46). Thus, our results re-emphasized the critical role of proprioceptive neurons in steering the re-organisation of neural pathways that supports functional recovery after SCI.

However, few studies have systematically investigated the impact of task-specific rehabilitation strategies prior to SCI on neuroplasticity and functional recovery. One study demonstrated that voluntary exercise prior to peripheral nerve injury enhances peripheral nerve regeneration (17). This observation is consistent with the robust axon regeneration resulting from an exposure to EE prior to a peripheral nerve injury. The study by Molteni et al reported an increase in neurotrophin mRNA in the DRG after exercise (17). Consequently, they used a pharmacological inhibitor of Trk tyrosine kinase to demonstrate that the exercise-mediated increase in DRG outgrowth was contingent on neurotrophin release. These findings differ from our data, since we did not observe any significant increase in neurotrophin mRNA or protein levels in DRGs after exposure to an EE. Along the same lines, a recent study has shown that exercise after SCI does not change neurotrophin expression in large-diameter DRG neurons (47). It is possible that the pharmacological inhibitor of Trk tyrosine kinase may have off-target effects altering multiple intracellular signalling pathways that lead to the reduction in DRG outgrowth. Voluntary exercise has been demonstrated to prevent the reduction of key signalling molecules that are involved in neuroplasticity including p-synapsin I, p-CREB and p-CaMK in the spinal cord and brain (48). Similarly, we found that EE triggers an increase in calcium related signalling molecules known to be important in gene regulation and inducing neuroplasticity. Involuntary exercise was recently shown to promote axon regeneration of propriospinal neurons but not sensory DRGs after a complete transection of the spinal cord and peripheral nerve graft (PNG) (49). This suggests that unlike the CBP activator used in the present study, increasing the activity of DRG neurons after a SCI using an exercise paradigm may be insufficient to increase the intrinsic regenerative state of the DRGs and promote sensory axon regeneration. Additionally, while we did not combine the CBP activator with

neurorehabilitation paradigms, this is worth investigating in the future since they might synergize for improved axonal plasticity and functional recovery.

Finally, it is worth speculating upon the anecdotal evidence that individuals who had an “active lifestyle” recover to a greater degree after SCI than individuals who lived “less active” lifestyles. In addition to the global benefits associated with a healthy lifestyle, our combined observations prompt us to suggest that neurons are “primed” for axonal regeneration and sprouting, which contribute to this enhanced recovery. It will be useful to collect epidemiological data supporting or refuting this hypothesis.

In summary, we have demonstrated an epigenetic-based mechanism underlying activity-dependent neuronal plasticity. The exploitation of this mechanism allowed us to utilize a novel pharmacotherapy that enhanced spinal cord repair and functional recovery after SCI, opening a realistic pathway for clinical evaluations.

## Materials and methods

Fig. S1 Exposure to EE enhances neurite outgrowth on inhibitory myelin substrate to a similar extent as a conditioning SNA injury

Fig. S2 Inhibiting transcription with actinomycin-D blocks the EE-mediated increase in DRG neurite outgrowth

Fig. S3. Exposure to EE enhances axon elongation rather than branching

Fig. S4. The full EE increases DRG neurite outgrowth compared to the running wheel alone

Fig. S5. Exposure to EE enhances muscle re-innervation by proprioceptive DRG neurons

Fig. S6. EE promotes axon regeneration and the formation of putative synapses

Fig. S7. Neurotrophin and cytokine levels in the DRG and blood serum are not affected by EE

Fig. S8. RNAseq and proteomic datasets demonstrate that EE strongly modulates pathways involved in neuronal activity, calcium signaling, gene expression and cytoskeletal changes

Fig. S9. Efficient transduction and DREADD expression in parvalbumin positive DRGs

Fig. S10. The EE-mediated increase in DRG neurite outgrowth is mediated by neuronal activity

Fig. S11. H3K27ac is increased in parvalbumin positive DRGs after exposure to EE but the levels of H3K4me2, H3K9ac and H3K4me3 do not change compared to SH

Fig. S12. Levels of H4K8ac but not acCBP or pCREB remain elevated in parvalbumin positive DRGs for 5 weeks after exposure to EE

Fig. S13. Increasing neuronal activity augments the level of H4K8ac and acCBP in DRG neurons

Fig. S14. The CaMKIIa promoter is active in DRG neurons and drives strong expression of tdTomato after tamoxifen treatment

Fig. S15. CSP-TTK21 treatment significantly enhances the time to remove adhesive tape placed on the hindpaw

Fig. S16. CSP-TTK21 treatment promotes sprouting of afferent fibres below the level of injury

Fig. S17. CSP-TTK21 treatment enhances H4K8ac in the DRG

Fig. S18. CSP-TTK21 treatment does not affect the glial scar after a thoracic dorsal spinal cord hemisection in mice

Fig. S19. CSP-TTK21 significantly reduced the number of slips during locomotion along a horizontal ladder

Fig. S20. CSP-TTK21 treatment enhances levels of H4K8ac in the raphe nucleus and reticular formation

Fig. S21. CSP-TTK21 treatment does not affect the glial scar after a thoracic contusion spinal cord injury in rats

Table S1. Table compiling the 78 parameters used for quantifying gait features.

Video S1. EE mediated calcium mobilization in proprioceptive DRG neurons

Video S2. SH mediated calcium mobilization in proprioceptive DRG neurons

Video S3. Treatment with CSP-TTK21 enhances hindlimb function and over-ground locomotion

File S1. WholeDRG\_EEvS StHousing DE  
 File S2. LDN\_EEvS StHousing DE  
 File S3. DE Proteins EEvS StHousing  
 File S4. LDN\_EEvS SHUpregulated  
 File S5. LDN\_GO and KEGG  
 File S6. ClueGO Result clustering\_LDN  
 File S7. ClueGO Result clustering\_LDN\_selected for STRINGbis

## References

1. M. V. Sofroniew, Dissecting spinal cord regeneration. *Nature* **557**, 343-350 (2018).
2. Z. He, Y. Jin, Intrinsic Control of Axon Regeneration. *Neuron* **90**, 437-451 (2016).
3. S. Di Giovanni, Molecular targets for axon regeneration: focus on the intrinsic pathways. *Expert Opin Ther Targets* **13**, 1387-1398 (2009).
4. F. Xie, B. Zheng, White matter inhibitors in CNS axon regeneration failure. *Exp Neurol* **209**, 302-312 (2008).
5. W. Plunet, B. K. Kwon, W. Tetzlaff, Promoting axonal regeneration in the central nervous system by enhancing the cell body response to axotomy. *J Neurosci Res* **68**, 1-6 (2002).
6. W. D. Snider, F. Q. Zhou, J. Zhong, A. Markus, Signaling the pathway to regeneration. *Neuron* **35**, 13-16 (2002).
7. I. G. McQuarrie, B. Grafstein, M. D. Gershon, Axonal regeneration in the rat sciatic nerve: effect of a conditioning lesion and of dbcAMP. *Brain Res* **132**, 443-453 (1977).
8. P. M. Richardson, V. M. Issa, Peripheral injury enhances central regeneration of primary sensory neurones. *Nature* **309**, 791-793 (1984).
9. S. Neumann, C. J. Woolf, Regeneration of dorsal column fibers into and beyond the lesion site following adult spinal cord injury. *Neuron* **23**, 83-91 (1999).
10. T. Akay, W. G. Tourtellotte, S. Arber, T. M. Jessell, Degradation of mouse locomotor pattern in the absence of proprioceptive sensory feedback. *Proc Natl Acad Sci U S A* **111**, 16877-16882 (2014).
11. A. Takeoka, I. Vollenweider, G. Courtine, S. Arber, Muscle spindle feedback directs locomotor recovery and circuit reorganization after spinal cord injury. *Cell* **159**, 1626-1639 (2014).
12. L. Asboth *et al.*, Cortico-reticulo-spinal circuit reorganization enables functional recovery after severe spinal cord contusion. *Nat Neurosci* **21**, 576-588 (2018).
13. E. Formento *et al.*, Electrical spinal cord stimulation must preserve proprioception to enable locomotion in humans with spinal cord injury. *Nat Neurosci*, (2018).
14. R. van den Brand *et al.*, Restoring voluntary control of locomotion after paralyzing spinal cord injury. *Science* **336**, 1182-1185 (2012).
15. F. B. Wagner *et al.*, Targeted neurotechnology restores walking in humans with spinal cord injury. *Nature* **563**, 65-71 (2018).
16. S. Neumann, F. Bradke, M. Tessier-Lavigne, A. I. Basbaum, Regeneration of sensory axons within the injured spinal cord induced by intraganglionic cAMP elevation. *Neuron* **34**, 885-893 (2002).
17. R. Molteni, J. Q. Zheng, Z. Ying, F. Gomez-Pinilla, J. L. Twiss, Voluntary exercise increases axonal regeneration from sensory neurons. *Proc Natl Acad Sci U S A* **101**, 8473-8478 (2004).
18. A. S. Wahl *et al.*, Neuronal repair. Asynchronous therapy restores motor control by rewiring of the rat corticospinal tract after stroke. *Science* **344**, 1250-1255 (2014).
19. W. G. Tourtellotte, J. Milbrandt, Sensory ataxia and muscle spindle agenesis in mice lacking the transcription factor Egr3. *Nat Genet* **20**, 87-91 (1998).
20. B. R. Ickes *et al.*, Long-term environmental enrichment leads to regional increases in neurotrophin levels in rat brain. *Exp Neurol* **164**, 45-52 (2000).
21. L. Rattazzi *et al.*, Impact of Enriched Environment on Murine T Cell Differentiation and Gene Expression Profile. *Front Immunol* **7**, 381 (2016).
22. A. L. Bombeiro *et al.*, Enhanced Immune Response in Immunodeficient Mice Improves Peripheral Nerve Regeneration Following Axotomy. *Front Cell Neurosci* **10**, 151 (2016).
23. B. L. Roth, DREADDs for Neuroscientists. *Neuron* **89**, 683-694 (2016).
24. Q. Jin *et al.*, Distinct roles of GCN5/PCAF-mediated H3K9ac and CBP/p300-mediated H3K18/27ac in nuclear receptor transactivation. *EMBO J* **30**, 249-262 (2011).
25. R. A. Henry, Y. M. Kuo, A. J. Andrews, Differences in specificity and selectivity between CBP and p300 acetylation of histone H3 and H3/H4. *Biochemistry* **52**, 5746-5759 (2013).
26. S. C. Hu, J. Chrivia, A. Ghosh, Regulation of CBP-mediated transcription by neuronal calcium signaling. *Neuron* **22**, 799-808 (1999).
27. J. C. Chrivia *et al.*, Phosphorylated CREB binds specifically to the nuclear protein CBP. *Nature* **365**, 855-859 (1993).



28. J. M. Alarcon *et al.*, Chromatin acetylation, memory, and LTP are impaired in CBP<sup>+/-</sup> mice: a model for the cognitive deficit in Rubinstein-Taybi syndrome and its amelioration. *Neuron* **42**, 947-959 (2004).
29. J. P. Lopez-Atalaya *et al.*, CBP is required for environmental enrichment-induced neurogenesis and cognitive enhancement. *EMBO J* **30**, 4287-4298 (2011).
30. P. R. Thompson *et al.*, Regulation of the p300 HAT domain via a novel activation loop. *Nat Struct Mol Biol* **11**, 308-315 (2004).
31. L. W. Yuan, A. Giordano, Acetyltransferase machinery conserved in p300/CBP-family proteins. *Oncogene* **21**, 2253-2260 (2002).
32. M. L. Bangaru *et al.*, Differential expression of CaMKII isoforms and overall kinase activity in rat dorsal root ganglia after injury. *Neuroscience* **300**, 116-127 (2015).
33. S. Chatterjee *et al.*, A novel activator of CBP/p300 acetyltransferases promotes neurogenesis and extends memory duration in adult mice. *J Neurosci* **33**, 10698-10712 (2013).
34. J. H. Lim *et al.*, Neural activity promotes long-distance, target-specific regeneration of adult retinal axons. *Nat Neurosci* **19**, 1073-1084 (2016).
35. P. B. Jaiswal, A. W. English, Chemogenetic enhancement of functional recovery after a sciatic nerve injury. *Eur J Neurosci* **45**, 1252-1257 (2017).
36. A. Tedeschi, T. Nguyen, R. Puttagunta, P. Gaub, S. Di Giovanni, A p53-CBP/p300 transcription module is required for GAP-43 expression, axon outgrowth, and regeneration. *Cell Death Differ* **16**, 543-554 (2009).
37. P. Gaub *et al.*, HDAC inhibition promotes neuronal outgrowth and counteracts growth cone collapse through CBP/p300 and P/CAF-dependent p53 acetylation. *Cell Death Differ* **17**, 1392-1408 (2010).
38. P. Gaub *et al.*, The histone acetyltransferase p300 promotes intrinsic axonal regeneration. *Brain* **134**, 2134-2148 (2011).
39. R. Puttagunta *et al.*, P/CAF-dependent epigenetic changes promote axonal regeneration in the central nervous system. *Nat Commun* **5**, 3527 (2014).
40. Y. Cho, V. Cavalli, HDAC5 is a novel injury-regulated tubulin deacetylase controlling axon regeneration. *EMBO J* **31**, 3063-3078 (2012).
41. Y. Cho, R. Sloutsky, K. M. Naegle, V. Cavalli, Injury-induced HDAC5 nuclear export is essential for axon regeneration. *Cell* **155**, 894-908 (2013).
42. S. Rossignol, A. Frigon, Recovery of locomotion after spinal cord injury: some facts and mechanisms. *Annu Rev Neurosci* **34**, 413-440 (2011).
43. H. R. Sandrow-Feinberg, J. D. Houle, Exercise after spinal cord injury as an agent for neuroprotection, regeneration and rehabilitation. *Brain Res* **1619**, 12-21 (2015).
44. M. L. Starkey *et al.*, High-Impact, Self-Motivated Training Within an Enriched Environment With Single Animal Tracking Dose-Dependently Promotes Motor Skill Acquisition and Functional Recovery. *Neurorehabil Neural Repair* **28**, 594-605 (2014).
45. Y. Q. Jiang, B. Zaaimi, J. H. Martin, Competition with Primary Sensory Afferents Drives Remodeling of Corticospinal Axons in Mature Spinal Motor Circuits. *J Neurosci* **36**, 193-203 (2016).
46. E. M. Moraud *et al.*, Mechanisms Underlying the Neuromodulation of Spinal Circuits for Correcting Gait and Balance Deficits after Spinal Cord Injury. *Neuron* **89**, 814-828 (2016).
47. B. E. Keeler *et al.*, Acute and prolonged hindlimb exercise elicits different gene expression in motoneurons than sensory neurons after spinal cord injury. *Brain Res* **1438**, 8-21 (2012).
48. F. Gomez-Pinilla, Z. Ying, Y. Zhuang, Brain and spinal cord interaction: protective effects of exercise prior to spinal cord injury. *PLoS One* **7**, e32298 (2012).
49. R. Sachdeva, C. C. Theisen, V. Ninan, J. L. Twiss, J. D. Houle, Exercise dependent increase in axon regeneration into peripheral nerve grafts by propriospinal but not sensory neurons after spinal cord injury is associated with modulation of regeneration-associated genes. *Exp Neurol* **276**, 72-82 (2016).
50. J. D. Kocsis, S. G. Waxman, Absence of potassium conductance in central myelinated axons. *Nature* **287**, 348-349 (1980).
51. H. Tanaka, K. Ono, H. Shibasaki, T. Isa, K. Ikenaka, Conduction properties of identified neural pathways in the central nervous system of mice in vivo. *Neurosci Res* **49**, 113-122 (2004).
52. C. Kathe, T. H. Hutson, S. B. McMahon, L. D. Moon, Intramuscular Neurotrophin-3 normalizes low threshold spinal reflexes, reduces spasms and improves mobility after bilateral corticospinal tract injury in rats. *Elife* **5**, (2016).
53. I. Rishal, M. Rozenbaum, M. Fainzilber, Axoplasm isolation from rat sciatic nerve. *J Vis Exp*, (2010).

**Acknowledgments:** We thank Marilyn Scandaglia from the Instituto de Neurociencias, Universidad Miguel Hernandez Consejo Superior de Investigaciones Científicas, Alicante, Spain for the images of Cre-driven expression of tdTomato in CaMKIIa positive DRG neurons.

**Funding:** This work was supported by grants from the Rosetrees Trust, Leverhulme Trust, Henry Smith Charity; start-up funds from the Division of Brain Sciences, Imperial College London (SDG); Wings for Life (SDG and LDFM); International Spinal Research Trust (LDFM and CK). The research was supported by the National Institute for Health Research (NIHR) Imperial Biomedical Research Centre (SDG). Research in the Lemmon/Bixby laboratory is supported by the Miami Project to Cure Paralysis, The Walter G. Ross Foundation, and NIH R01 HD057632. Research in the Barco lab is supported by grants SAF2014-56197-R, PCIN-2015-192-C02-01 and SEV-2013-0317 from the Spanish Ministry of Economy and Competitiveness (MINECO) co-financed by the European Regional Development Fund (ERDF), a NARSAD Independent Investigator Grant from the Brain & Behavior Research Foundation and a grant from the Alicia Koplowitz Foundation. The Instituto de Neurociencias is a “Centre of Excellence Severo Ochoa”. Research in the Courtine lab was supported by a Consolidator Grant from the European Research Council [ERC-2015-CoG HOW2WALKAGAIN 682999] and the Swiss National Science Foundation (subsidy 310030B\_166674 and CRSII3\_160696). TKK is a recipient of Sir J C Bose Fellowship’. Muthusamy Eswaramoorthy of Nanomaterials and Catalysis Laboratory, Chemistry and Physics of Materials Unit, JNCASR, Banaglore, India for technical help.

**Author contributions:** THH, CK, GC and SDG conceived and supervised the studies. THH, IP, AH, FDV, LM performed, collected and analysed data from WT mice. THH, AMF, JLA and AB collected and analysed the data from CaMKIIa-creERT2/CBP<sup>f/f</sup> mice. THH, KB and QB collected and analysed the data from PV-cre x GCaMP, PV-cre x tdTomato and *Egr3*<sup>-/-</sup> mice. IP, MCD, JLB and VPL performed, collected and analysed the laser capture and RNAseq. LZ, GK and IP, collected and analysed the proteomics. ALB, SHS, AKS, PC, and TKK developed and synthesized the CBP-TTK21 compound. THH, CK, KB and QB collected and analyzed the data in rats. THH, CK and KB prepared the figures. THH, GC and SDG wrote the manuscript and all the authors contributed to its editing.

**Competing interests:** TKK holds the following patents related to CSP-TTK21. (a) International Patent: PCT/IN2008/000632. Title of the invention: Intrinsically Fluorescent Carbon Nanospheres and a Process thereof. (b) US Patent WO2013160885 A1, US20150119466, European Patent EP2841111 A1. Title of the invention: Nanosphere-Histone Acetyltransferase (HAT) Activator Composition. process and methods thereof. (c) USS Patent:US93145399B2. Title of the invention: Nanosphere-histone acetyltransferase (HAT) activator composition, process and methods thereof. Otherwise the authors declare no competing interests.

**Data and material availability:** Proteomics data are available as PeptideAtlas dataset submission PASS0132. Gene expression RNAseq data are available on GEO repository, GSE125793.

**Figure. 1. Environmental enrichment induces a lasting increase in the regenerative potential of sensory neurons.** **a**, Cultured mouse sciatic DRGs after exposure to EE, stained for Beta-III-tubulin. Scale bar 100  $\mu$ m. **b**, Quantification of neurite outgrowth (mean  $\pm$  SEM, Unpaired Student’s t-tests \*\*\*P<0.001, n = 4/group). **c**, Diagram illustrating the experimental design, sciatic DRGs were cultured from mice that had been placed in EE for 10 days and then returned to SH for up to 5 weeks. **d**, Example images of sciatic DRGs from mice that had been in SH or EE for 10 days and then SH for 5 weeks. Scale bar 100  $\mu$ m. **e**, Quantification of neurite outgrowth indicated that DRGs from mice that had been exposed to EE still had significantly increased neurite outgrowth compared to SH controls (mean  $\pm$  SEM, unpaired Student’s t test \*\*\* P<0.001, n = 4/group). **f**, Sciatic nerves immunostained for SCG10 after transection and re-anastomosis, Scale bar 500  $\mu$ m. **g**, Quantification of regenerating axons (mean  $\pm$  SEM, Two-

way ANOVA, Holm-Sidak post-hoc, \*\*\* $P < 0.001$ , \*\* $P < 0.01$ , \* $P < 0.05$   $n = 6/\text{group}$ ). **h**, CTB-traced (red) dorsal column axons after injury, DAPI (blue), lesion site (dashed line). Scale bar, 200  $\mu\text{m}$ . **i**, Quantification of CTB positive regenerating axons (mean  $\pm$  SEM, Two-way repeated measures ANOVA, Tukey's post-hoc \*\* $P < 0.01$ , \*\*\* $P < 0.001$ ,  $n = 10/\text{group}$ ). **j**, Electrophysiological setup. **k**, Compound action potentials recorded below (blue) and above (black) injury. **l**, Quantification of compound action potentials above the lesion (mean  $\pm$  SEM, One-way ANOVA, Fisher's LSD post-hoc \*\*\* $P < 0.001$ ,  $n = 6/\text{group}$ ).

**Figure. 2. Proprioceptive afferent feedback is required for EE-mediated increase in DRG regenerative growth.** **a**, Schematic of the experimental design, after EE and SH exposure mice underwent sciatic nerve crush injury and CTB injection distal to the crush site, axons that regenerate across the injury site take up CTB and retrogradely transport it to the soma. **b**, Representative images of co-localization between parvalbumin, substance P or isolectin B4 (green) and CTB (red) in DRGs from EE mice that had undergone a sciatic nerve crush. Scale bar, 50  $\mu\text{m}$ . **c**, Quantification of the number of CTB positive DRG neurons suggests EE significantly enhances axon regeneration compared to SH (mean  $\pm$  SEM, unpaired Student's  $t$  test, \*\*  $P < 0.01$ ,  $n = 3/\text{group}$ ). **d**, Quantification of the percentage of CTB positive neurons that co-localized with parvalbumin, substance P or isolectin B4 demonstrates high levels of co-localization between CTB and parvalbumin after exposure to EE. **e**, Schematic showing *Egr3* mutation resulting in degeneration of muscle spindles. **f**, Beta-III-tubulin stained sciatic DRGs from WT or *Egr3*<sup>-/-</sup> mice after exposure to SH or EE. Scale bar 100  $\mu\text{m}$ . **g**, Quantification of neurite outgrowth. (mean  $\pm$  SEM, One-way ANOVA, Tukey's post-hoc, \*\*\* $P < 0.001$ ,  $n = 4/\text{group}$ ). **h**, Example images of tdTomato (red) positive or tdTomato negative DRGs co-stained with beta-III-tubulin (green) cultured from PV-cre x tdTomato mice that had been exposed to either SH or EE for 10 days. Scale bar 100  $\mu\text{m}$ . **i**, Quantification of neurite outgrowth showed EE significantly increased outgrowth of PV-tdTomato+ DRGs compared to PV-tdTomato- DRGs (mean  $\pm$  SEM, One-way ANOVA, Tukey's post-hoc, \*\*  $P < 0.01$ , \*\*\*  $P < 0.001$ ,  $n = 5/\text{group}$ ).

**Figure. 3. EE induces signaling pathways involved in neuronal activity, calcium mobilization and the regenerative program of large-diameter DRG neurons.** **a**, Heatmap of the differentially expressed (DE) genes in whole-DRG and LDN RNA-seq ( $P < 0.05$ ). Color scale represents arbitrary expression units (lowest, blue; highest, red). **b**, Pie chart of genes in each functional group identified by GO analysis of DE genes in LDN. Functional groups are color-coded. **c**, Sciatic nerves transduced with AAV5-GFP, AAV5-hM4Di-mCitrine or AAV5-hM3Dq-mCitrine labeled with mCitrine/GFP after sciatic nerve crush. Arrow-head: lesion site. Scale bar, 500  $\mu\text{m}$ . **d**, Quantification of axon regeneration (mean  $\pm$  SEM, Two-way repeated measures ANOVA, Tukey's post-hoc, \*\*\* $P < 0.001$ ,  $n = 6/\text{group}$ ). **e**, Time-lapse images of intracellular calcium release from whole-mount PV-GCaMP DRGs before and after addition of 150 mM KCL. Scale bar, 50  $\mu\text{m}$ . **f**, Quantification of F/Fo ratio after 50 mM, 100 mM and 150 mM KCl (mean  $\pm$  SEM, Two-way ANOVA, Sidak's post-hoc \*\* $P < 0.01$ , \*\*\* $P < 0.001$ ,  $n = 4/\text{group}$ ).

**Figure. 4. CBP is required for EE-dependent increase in regeneration potential.** **a**, DRGs stained for H4K8ac (green), parvalbumin (red) and DAPI (blue). Scale bar, 50  $\mu\text{m}$ . **b**, Quantification of H4K8ac intensity (mean  $\pm$  SEM, unpaired Student's  $t$  test \*\*\*  $P < 0.001$ ,  $n = 6/\text{group}$ ). **c**, Examples images of DRGs from mice housed in SH or EE, which were double stained for pCREB (green) and parvalbumin (red). Scale bar, 50  $\mu\text{m}$ . **d**, Quantification of the fluorescence intensity of pCREB in the nuclei of parvalbumin positive DRGs show as significant increase 10 days after EE compared to SH (mean  $\pm$  SEM, unpaired Student's  $t$  test \*\*\*  $P < 0.001$ ,  $n = 4/\text{group}$ ). **e**, Immunoblotting analysis for H4K8ac from protein extracts from whole sciatic DRGs after 10 days exposure to SH or EE. Shown is a significant increase in the

expression of H4K8ac following exposure to EE (mean  $\pm$  SEM, unpaired Student's t test, \*\*  $P < 0.01$ ,  $n = 3/\text{group}$ ). H4K8ac was normalised the levels of H4, while GAPDH was used as a loading control. **f**, Immunoblotting analysis for pCREB from protein extracts of whole sciatic DRGs revealed that exposure to EE significantly increased levels of pCREB compared to SH (mean  $\pm$  SEM, unpaired Student's t test \*\*  $P < 0.01$ ,  $n = 3/\text{group}$ ). pCREB was normalised to levels of CREB, while GAPDH was used as a loading control. **g**, DRGs stained for acCBP (green) and total CBP (red). Scale bar, 50  $\mu\text{m}$ . **h**, Quantification of acCBP intensity (mean  $\pm$  SEM, unpaired Student's t test \*\*\*  $P < 0.001$ ,  $n = 11/\text{group}$ ). **i**, Cultured DRG neurons from WT x CBP<sup>f/f</sup> or CaMKIIa-creERT2 x CBP<sup>f/f</sup> mice (Beta-III-tubulin, red and H4K8ac, green). Scale bar, 200  $\mu\text{m}$ . **j**, Quantification of neurite outgrowth (mean  $\pm$  SEM, One-way ANOVA, Tukey's post-hoc \*\*\*  $P < 0.001$ ,  $n = 5/\text{group}$ ). **k**, Quantification of H4K8ac intensity (mean  $\pm$  SEM, One-way ANOVA, Tukey's post-hoc \*\*\*  $P < 0.001$ ,  $n = 5/\text{group}$ ).

**Figure 5. Pharmacological activation of CBP/p300 promotes sensory axon regeneration and recovery after a dorsal hemisection SCI in mice.** **a**, Cultured DRG neurons treated with control (CSP) or CBP/p300 pharmacological activator (CSP-TTK21) (Beta-III-tubulin, red and H4K8ac, green). Scale bar, 50  $\mu\text{m}$ . **b**, Quantification of neurite outgrowth (mean  $\pm$  SEM, unpaired Student's t test \*\*  $P < 0.01$ ,  $n = 4/\text{group}$ ), H4K8ac intensity (mean  $\pm$  SEM, unpaired Student's t test \*\*  $P < 0.01$ ,  $n = 4/\text{group}$ ) and neurite branching (mean  $\pm$  SEM, unpaired Student's t test \*  $P < 0.05$ ,  $n = 4/\text{group}$ ). **c**, T9 dorsal column axotomy lesions ascending sensory axons in the dorsal columns. **d**, CTB (red) was injected into the sciatic nerve 5 weeks after SCI. **e**, CTB-traced (red) dorsal column axons after SCI, GFAP (green), DAPI (blue), lesion site (dashed line). Scale bar, 200  $\mu\text{m}$ . **f**, Quantification of CTB positive regenerating axons (mean  $\pm$  SEM, Two-way repeated measures ANOVA, Holm's Sidak post-hoc \*\*\*  $P < 0.001$ , \*\*  $P < 0.01$ , \*  $P < 0.05$ ,  $n = 8/\text{group}$ ). **g**, Quantification of slips (mean  $\pm$  SEM, Two-way repeated measures ANOVA, Fisher's LSD post-hoc \*  $P < 0.05$ ,  $n = 8/\text{group}$ ). **h**, Quantification of the time it took to first contact an adhesive pad placed on the hindpaws (mean  $\pm$  SEM, Two-way repeated measures ANOVA, Fisher's LSD post-hoc \*\*\*  $P < 0.001$ , \*\*  $P < 0.01$ , \*  $P < 0.05$ ,  $n = 8/\text{group}$ ). **i**, Representative image from a control CSP treated mouse showing very few CTB-positive regenerating axons rostral to the lesion and little co-localization with the pre-synaptic marker vGlut1. Lesion site is marked by the dashed line and asterisk. Scale bar, 100  $\mu\text{m}$ , scale bar for insets 10  $\mu\text{m}$ . **j**, Representative image from a CSP-TTK21 treated mouse showing co-localization of regenerating CTB (red) positive axons rostral to the spinal cord injury site (marked by the dashed line and asterisks) with the pre-synaptic marker vGlut1 (green) to identify prospective nascent synapses (marked by arrows). Scale bar, 100  $\mu\text{m}$ . Higher-magnification images of insets show co-localization of CTB positive axons (red) and vGlut1 (green). Scale bar, 10  $\mu\text{m}$ . **k**, Compound action potentials recorded below (grey) and above (black) the lesion. **l**, Quantification of compound action potentials above the lesion (mean  $\pm$  SEM, unpaired Student's t test \*\*  $P < 0.01$ ,  $n = 8/\text{group}$ ). **m**, vGluT1 positive boutons (white) from Group-Ia afferents in proximity to hindlimb motoneurons (Red, CTB) below the injury (L1-4). Scale bar, 25  $\mu\text{m}$ . **n**, Quantification of vGluT1 positive boutons opposed to motoneurons (mean  $\pm$  SEM, unpaired Student's t test \*\*  $P < 0.01$ ,  $n = 8/\text{group}$ ).

**Figure 6. Pharmacological CBP/p300 activation enhances sprouting of both descending motor and ascending sensory axons leading to functional recovery after contusion SCI in rats.** **a**, Image showing joints used for reconstruction of hindlimb movements **b**, Representative hindlimb kinematics after treatment with CSP or CSP-TTK21. Black, orange and grey correspond to stance, drag and swing phases of gait, respectively. **c**, PC analysis of gait parameters averaged for each group at weeks 1, 4 and 8 and quantification of average scores on PC1, which quantify the locomotor performance of rats treated with CSP or CSP-TTK21 (mean  $\pm$  SEM, Two-way ANOVA, Fisher's LSD post-hoc \*  $P < 0.05$ ,  $n = 10/\text{group}$ ). **d**, Bar plots of drag duration and step height show significant improvements after CSP-TTK21

treatment (mean  $\pm$  SEM, unpaired Student's *t* test \*  $P < 0.05$ , \*\* $P < 0.01$ ,  $n = 10/\text{group}$ ). **e**, Schematics showing strategy for tracing vGi axons, T9 contusion and the L4 ventral horn analyzed for vGi and 5HT sprouting. **f**, CSP-TTK21 increased sprouting of descending vGi axons (Red) observed around motoneurons (ChAT, Cyan) in the lumbar ventral horn. Scale bar, 50  $\mu\text{m}$ . **g**, Quantification of vGi intensity in the ventral horn (mean  $\pm$  SEM, unpaired Student's *t* test, \*\*\* $P < 0.001$ ,  $n = 10/\text{group}$ ). **h**, CSP-TTK21 increased sprouting of descending 5HT axons (Magenta) was observed around motoneurons (ChAT, Cyan) in the lumbar ventral horn. Scale bar, 50  $\mu\text{m}$ . **i**, Quantification of 5HT intensity in the ventral horn (mean  $\pm$  SEM, unpaired Student's *t* test, \*\*\* $P < 0.001$ ,  $n = 10/\text{group}$ ). **j**, Sagittal sections showing CSP-TTK21 increased sprouting of descending vGi (Red) and 5HT (Green) axons around motoneurons (ChAT, White) below in the injury in the lumbar ventral horn. Scale bar, 50  $\mu\text{m}$ . **k**, vGluT1 positive boutons (yellow) from Group-Ia afferents in proximity to motoneurons (ChAT, Cyan) below the injury (L1-4). Scale bar, 25  $\mu\text{m}$ . **l**, Quantification of vGluT1 positive boutons opposed to motoneurons (mean  $\pm$  SEM, unpaired Student's *t* test \*\*\* $P < 0.001$ ,  $n = 10/\text{group}$ ). **m**, The amplitude of the H-wave significantly increased after treatment with CSP-TTK21 (mean  $\pm$  SEM, One-way ANOVA, Tukey's post-hoc \*  $P < 0.05$ ,  $n = 10/\text{group}$ ).

## Materials and Methods

### Study design

We investigated the impact of environmental enrichment (EE) on proprioceptive DRG neurons, hypothesizing that EE would prime these neurons to initiate a regenerative response to a subsequent injury. Augmenting the activity of proprioceptive DRG neurons using EE induces and is required for an increase in neurite outgrowth and axon regeneration that is dependent on CREB Binding Protein (CBP)-mediated histone acetylation. In turn, pharmacologically increasing CBP acetyltransferase activity at clinically-relevant times and in clinically-relevant models of spinal cord injury promoted regeneration and sprouting of sensory and brainstem motor axons that mediated improvements in both sensory and motor function. All surgical and experimental procedures on rodents were carried out in accordance with the UK Animals (Scientific Procedures) Act 1986 and approved by the veterinarian and ethical committee of Imperial College and the canton of Vaud and Geneva. Animals were assigned randomly to experimental groups and surgeries were carried out in a random block design. All analysis was performed by the same experimenter who was blinded to the experimental groups. All behavioral testing and analysis was performed by an observer blinded to the experimental groups. *N* values represent the number of animals in the experiment and each experiment contained a minimum of 3 technical replicates. Behavioral assays were replicated two or three times per time-point, depending on the experiment.

### Animal models

All procedures were carried out in accordance with the UK Animals (Scientific Procedures) Act 1986 and approved by the veterinarian and ethical committee of Imperial College and the canton of Vaud and Geneva. Male C57BL/6J mice (Charles River Laboratories, UK) ranging from 6 to 8 weeks of age were used for all experiments except those specifying transgenic mice. Female WT/lox-tdTomato, CaMKIIa-Cre-ERT2/lox-tdTomato, CaMKIIa-Cre-ERT2/CBP<sup>f/f</sup>, WT/CBP<sup>f/f</sup> mice with a C57BL/6J genetic background have been previously described(29). For CBP ablation experiments, tamoxifen (T5648; Sigma) was administered to 4 week old CaMKIIa-creERT2/CBP<sup>f/f</sup> mice using a gastric probe for 5 consecutive days (total consumption ~20 mg per animal); control animals were non-cre recombinase expressing CBP<sup>f/f</sup> mice (WT/CBP<sup>f/f</sup>) treated with tamoxifen. PV-cre x GCaMP and PV-cre x tdTomato mice on a C57BL/6J genetic background were provided by the Courtine laboratory. *Egr3*<sup>-/-</sup> mice containing the *Egr3* mutant allele previously described(19) were maintained on a C57BL/6J

genetic background and provided by the Courtine lab. Adult female Lewis rats (180–220 g body weight, 14–30 weeks of age) were used for the CBP activator experiment.

### **Animal housing**

Animals were kept on a 12 hr light:dark cycle with food and water provided ad libitum. Standard housing for mice consisted of 26x12x18 cm<sup>3</sup> cages housing 4 mice with tissue paper for bedding, a tunnel and a wooden chewstick. The enriched environment housing consisted of 36x18x25 cm<sup>3</sup> cages housing 8 mice with tissue paper for bedding, a tunnel and a wooden chewstick. EE cages also received additional nesting material which included nestlets, rodent roll and sizzle pet (LBS biotech). EE cages continually contained a hanging plastic tunnel (LBS biotech) and a plastic igloo combined with a fast-track running wheel (LBS-biotech). In addition to this EE cages received a wooden object (cube, labyrinth, tunnel, corner 15) (LBS biotech) that was changed after 5 days to help maintain a novel environment. The EE cages also received 15 g fruity gems (LBS biotech) every 5 days to encourage exploratory and natural foraging behaviour. Rats were housed in standard housing conditions with 3 rats per cage.

### **DRG culture**

Glass coverslips were coated with 100 µg/ml poly-D-lysine (Invitrogen) in H<sub>2</sub>O for 2 hours at room temperature. The PDL was removed and washed 3 times with PBS (Invitrogen, UK), after which they were coated with 2 µg/ml of laminin (Millipore) for 2 hours at 37 °C. For the inhibitory myelin substrate, 8 µg/cm<sup>2</sup> of extracted rat myelin was added to the laminin coated coverslip for 2 hrs at room temperature before removing the myelin and leaving to air dry for 30 mins. L4-L6 DRGs were dissected and collected in Hank's balanced salt solution (HBSS) (Invitrogen) on ice. DRGs then underwent enzymatic digestion (5 mg/ml Dispase II (Sigma), 2.5 mg/ml Collagenase Type II (Worthington) in DMEM (Invitrogen) and incubated at 37 °C for 45 min with occasional mixing. DRGs were then transferred to media containing 10% heat-inactivated fetal bovine serum (Invitrogen, UK), B27 (Invitrogen) in DMEM:F12 (Invitrogen) mix and were briefly triturated with a 1 ml pipette to manually dissociate the DRG. After which, the single cell suspension was spun down, re-suspended in media containing 1x B27 and Penicillin/Streptomycin in DMEM:F12 mix and plated at 4,000 cells per coverslip and 4,500 per coverslip for the myelin substrate. The culture was maintained in a humidified incubator at 5% CO<sub>2</sub> and 37 °C for 12 or 24 hours before fixing with 4% PFA (Sigma) in PBS (Sigma). For the transcriptional inhibition experiment 0.01 µg/µl or 1 µg/µl Actinomycin-D was added to the culture media at time of DRG plating.

### **Immunocytochemistry**

Cultures were fixed with 4% PFA (Sigma) for 20 mins at room temperature and then washed with 1X PBS (Invitrogen). The cells were blocked with 10% normal donkey serum (Sigma) in PBS + 0.3% Triton-X for 1 hour at room temperature. Primary antibodies used were: Beta-III-tubulin (1:1000, Promega G712A) and H4K8ac (1:1000, Abcam ab15823). Primary antibodies were diluted in 10% normal donkey serum (Sigma) in PBS + 0.3% Triton-X and left incubating with the cells for 4 hours at 4 °C. Primary antibodies were removed and the cells washed 3 times in 1X PBS. This was followed by incubation with Alexa Fluor 568-conjugated Donkey anti-mouse and Alexa Fluor 488-conjugated Donkey anti-rabbit (1:1000, Invitrogen) in PBS + 0.3% Triton-X for 2 hours at room temperature. To visualize the nucleus, the cells were stained with DAPI (1:5000, Molecular Probes) in PBS + 0.3% Triton-X.

### **Sciatic nerve axotomy, crush and reanastomosis**

Mice were anaesthetised with 3% isoflurane in 1 L/min oxygen and given a subcutaneous injection of 5 mg/kg Rimadyl and 0.1 mg/kg Buprenorphine for perioperative analgesia. A small incision was performed at the gluteal region and the muscles bluntly dissected to expose the sciatic nerve. For SNA the sciatic nerve was completely transected using micro-scissors

(Fine Science Tools). For the crush injury the sciatic nerve was crushed using no.5 fine forceps (Fine Science Tools) keeping constant firm pressure for 10 seconds. For reanastomosis the nerve was completely transected as above and the two ends were re-anastomosed using two 2.0 sutures. The skin was then closed with two suture clips. For sham surgeries the sciatic nerve was exposed but left uninjured. Regeneration was assessed 1 day after the crush and 3 days after the reanastomosis.

### **Intramuscular injection**

Fourteen days post sciatic nerve crush sensory axons that had re-innervated the muscle were traced by injecting 5 µl of 1% CTB (List Biological Laboratories) diluted in saline into the tibialis anterior and medial gastrocnemius muscles using a 10 µl Hamilton syringe and Hamilton needle (NDL small RN ga34/15mm/pst45°) (Hamilton). 4 days post-tracing, mice were terminally anaesthetised and transcardially perfused with 20 ml PBS (pH 7.4) (Sigma) followed by 20 ml 4% paraformaldehyde in PBS (Sigma).

### **Dorsal hemisection injury**

Surgeries were performed as previously reported (39). Briefly, mice were anaesthetised with 3% isoflurane in 1 L/min oxygen and given a subcutaneous injection of 5 mg/kg Rimadyl and 0.1 mg/kg Buprenorphine for perioperative analgesia. A laminectomy at vertebra T9 was performed to expose spinal level T12 and a dorsal hemisection until the central canal was then performed using micro-scissors (Fine Science Tools). For the sham surgery a laminectomy was performed but the dorsal hemisection was not. Any bleeding was stopped and the muscle and skin was sutured closed.

**Contusion injury** Rats were anaesthetised with 3% isoflurane in 1 L/min oxygen, a partial laminectomy was made at the T9 vertebra. Contusion injury was produced using a force-controlled spinal cord impactor (IH-0400 Impactor, Precision Systems and Instrumentation). The applied force was set to 220 kdyn (1 dyn = 10 µN). The spinal cord displacement induced by the impact was measured for each animal. Analgesia (buprenorphine, 0.01–0.05 mg/kg, s.c.) and antibiotics (Baytril 2.5%, 5–10 mg/kg, s.c.) were provided for 3 days after surgery

### **Axonal tracing - Mice**

Six weeks post spinal cord injury the sensory axons in the dorsal columns were traced by injecting 3 µl of 1% CTB (List Biological Laboratories) diluted in saline into the sciatic nerve using a 10 µl Hamilton syringe and Hamilton needle (NDL small RN ga34/15mm/pst45°) (Hamilton). 4 days post-tracing, mice were terminally anaesthetised and transcardially perfused with 20 ml PBS (pH 7.4) (Sigma) followed by 20 ml 4% paraformaldehyde in PBS (Sigma).

To trace DRG neurons that regenerated an axon across a sciatic nerve crush, 2 µl of 1% CTB (List Biological Laboratories) diluted in saline was injected into the sciatic nerve 1 day after the crush injury using a 10 µl Hamilton syringe and Hamilton needle (NDL small RN ga34/15mm/pst45°) (Hamilton). 2 days post-tracing, mice were terminally anaesthetised and transcardially perfused with 20 ml PBS (pH 7.4) (Sigma) followed by 20 ml 4% paraformaldehyde in PBS (Sigma).

### **Axonal tracing - Rat**

Nine weeks post contusion injury an AAV vector was injected (AAV8-CAG-DIO-tdTomato-COMET, titre  $1.03 \times 10^{13}$  vg/ml, kindly provided by Prof. M. Tuszynski) into the ventral gigantocellular (vGi) for tract-tracing was performed in rats. Under isoflurane anesthesia, a craniotomy was performed over the brainstem medulla oblongata. Injection coordinates for rats were –11, –11.5, –12 mm caudal,  $\pm 0.8$  mm mediolateral to bregma and 9.5 mm ventral from the surface of the cerebellum (six injections total, 250 nl per injection, injected with a



Hamilton injection system). The AAV vector was injected at 3 nl/s and the needle was held in place for 3 min before being slowly retracted. Five weeks after the AAV injections rats were terminally anaesthetised and transcardially perfused with 200 ml PBS (pH 7.4) (Sigma) followed by 200 ml 4% paraformaldehyde in PBS (Sigma).

### **Histology and immunohistochemistry**

Tissue was post-fixed in 4% paraformaldehyde (PFA) (Sigma) and transferred to 30% sucrose (Sigma) overnight to cryoprotect, the tissue was then embedded in OCT compound (Tissue-Tek) and frozen at -80 °C. DRGs were sectioned at 10 µm thickness and mouse spinal cord at 15 µm, rat spinal cord at 30 µm and rat brainstem at 40 µm using a cryostat (Leica). Tissue sections were blocked for 1 h with 10% normal donkey serum (Sigma), 0.3% Triton X-100 (Sigma) in PBS, and then incubated with, and H4K8ac (1:1000, ab15823), H3K27ac (1:500, ab4729), H3K9ac (1:500, Cell Signalling 9671), H3K4me<sup>3</sup> (1:500, Abcam ab8580), H3K4me<sup>2</sup> (1:500, Cell signalling 9726), Parvalbumin (1:1000, Abcam ab64555), Substance P (1:250 ab67006), IB4 (1:250, Invitrogen 121411), CBP (1:50, Abcam ab50702), acCBP (1:1000, Abcam ab61242), pCREB (1:100, Abcam ab32096), SCG-10 (1:500, Novus biologicals NBP1-49461), CTB (1:1000, List biological 703), vGlut1 (1:1000, Synaptic system 135302), 5-HT (1:6000, Sigma S5545), ChAT (1:200 Chemicon AB144P), GFAP (1:500, Millipore AB5804) antibodies O/N. This was followed by incubation with Alexa Fluor 568-conjugated donkey anti-mouse and Alexa Fluor 488-conjugated donkey anti-rabbit or Alexa Fluor 568-conjugated donkey anti-rabbit and Alexa Fluor 488-conjugated donkey anti-mouse (1:1000, Invitrogen), respectively. Slides were counterstained with DAPI to visualise nuclei (1:5000, Molecular Probes). Photomicrographs were taken with a Nikon Eclipse TE2000 microscope with a optiMOS scMOS camera using 10x or 20x magnification.

### **Image analysis**

Image analysis was performed using ImageJ (Fiji) software. All analysis was performed by the same experimenter who was blinded to the experimental groups.

### **Analysis of neurite outgrowth**

The mean neurite outgrowth per DRG neuron was manually measured using the NeuronJ plugin for ImageJ. We measured the mean neurite outgrowth of 75 neurons per mouse with at least 4 mice per group and 3 technical replicates per mouse. The EE-mediated increase in DRG outgrowth was also independently verified by our collaborators in Miami (Lemmon/Bixby lab), strengthening the reproducibility of this phenotype.

### **Analysis of immunohistochemistry for epigenetic marks, pCREB, CBP and acCBP**

For quantitative analysis of pixel intensity, the nucleus or soma of DRG neurons were manually outlined in images from one series of stained tissue for each mouse. To minimise variability between images pixel intensity was normalized to an unstained area and the exposure time and microscope setting were fixed throughout the acquisition.

### **Analysis of vGi and 5HT fibres in the ventral horn**

Intensity of 5HT immunohistochemistry or tdTomato fluorescent protein labelling of the vGi fibres was measured in the ventral horn of L1-4 spinal sections. Quantification was done using ImageJ, the background was subtracted and then the mean pixel intensity was measured from one series of tissue for each animal.

### **Analysis of vGlut1 immunohistochemistry in proximity to motor neurons**



vGlut1, a pre-synaptic marker labelling proprioceptive or cutaneous sensory afferent terminals was used to identify boutons in close proximity to motor neurons, which had been retrogradely traced with CTB. To determine the number of vGlut1 boutons in close proximity to motor neurons, consecutive confocal images (0.3  $\mu\text{m}$  thick optical sections) were acquired as Z-stacks (total average thickness: 15  $\mu\text{m}$ ) using a 40x objective. The Average number of vGlut1 boutons opposed to motor neurons in the ventral horn of L1-3 spinal sections was calculated by analysing at least 20 motor neurons per animal.

### **Analysis of GFAP intensity and area around the lesion site**

GFAP intensity and area was quantified from sagittal spinal cord sections from one series of tissue for each animal. Quantification was done using ImageJ, the background was subtracted and then the mean pixel intensity and area of immune-reactivity was measured.

### **Analysis of CTB positive dorsal column axon regeneration in the spinal cord**

Regeneration of dorsal column axons were quantified from sagittal spinal cord sections from one series of tissue for each mouse. CTB intensity was quantified using ImageJ software at set distances rostral to injury centre then expressed as a percentage of the CTB intensity caudal to the injury site to control for variations in tracing efficacy.

The furthest rostral CTB positive axon was determined relative to the lesion centre and caudal axon retraction was defined as distance the lesioned axon bundle retracted relative to the lesion centre.

### **Analysis of SCG10 and mCitrine axon regeneration after sciatic nerve injury**

The regeneration of peripheral axons in the sciatic nerve was quantified from one series of tissue from each mouse. SCG10 or mCitrine intensity was quantified using ImageJ software at set distances distal to injury site then expressed as a percentage of the pixel intensity proximal to the injury site to control for variations in staining or transduction efficiency.

### **Behavioral analysis**

Mice were trained daily for 2 weeks pre-surgery before baseline measurements and then assessed on day 3 post-surgery and weekly thereafter. All behavioral testing and analysis was done by an observer blinded to the experimental groups.

**Gridwalk** – Mice crossed a 1 m long horizontal grid 3 times. Videos of the runs were analysed at a later time-point and errors from both hind-limbs were counted. Error values represent the total number of slips made by both hind-limbs over the 3 runs.

**Horizontal ladder** – Rats walked across a 1 m long horizontal ladder 3 times. Videos of the runs were analysed and errors from both hind-limbs were counted. Error values represent the total number of slips made by both hind-limbs over the 3 runs.

**Adhesive tape test** – An 8 mm diameter adhesive pad was placed on each hind-paw. The mouse was then placed into plexi-glass box and the time until it first made contact with each of the adhesive pads was recorded, followed by the time until it removed the adhesive pads from each hind-paw. The maximum time allowed for each animal was 5 mins. Each animal was tested twice per time-point and values represent the average time from both hindpaws from both runs.

## **Kinematic recordings**

All procedures used have been detailed previously (12, 14). Kinematic recordings were obtained from rats walking over-ground along a horizontal runway. Bilateral hindlimb kinematics were captured with a Vicon high-speed motion capture system (Vicon Motion Systems), using 12 infrared cameras (200 Hz). Reflective markers were attached bilaterally at the iliac crest, the greater trochanter (hip joint), the lateral condyle (knee joint), the lateral malleolus (ankle) and the distal end of the fifth metatarsophalangeal joint. The body was modeled as an interconnected chain of rigid segments, and joint angles were generated accordingly. For both the left and right legs, 10 step cycles were extracted randomly over several trials on the runway for each rat at each time point.

## **Analysis of kinematic recordings**

A total of 78 parameters quantifying gait features were computed for each leg and each gait or stroke cycle according to methods described in detail previously (12, 14). All parameters are reported in Supplementary Table 1. To evaluate differences between experimental conditions and groups, as well as the most relevant parameters to explain these differences, we implemented a multistep statistical procedure based on principal component (PC) analysis. PC analyses were applied to data from all individual gait cycles for all rats together. Data were analysed using the correlation method, which adjusts the mean of the data to 0 and the s.d. to 1. This method of normalization allows the comparison of variables with disparate values (large vs. small values) as well as different variances. Locomotor performance was quantified with the score along PC1, which segregated differences between groups. Factor loading of parameters on PC1, i.e. the correlations between each parameter and PC1 explaining recovery, are reported in Table S1.

## **Electrophysiology**

Mice were anaesthetized with an IP injection of 50 mg/kg ketamine and 0.5 mg/kg medetomidine. Their thoracic and lumbar back was shaved and disinfected with chlorhexidine. Mice were kept on a heating blanket throughout the procedure and anesthesia depth was monitored and the anaesthesia topped up if needed. Laminectomies were performed at vertebrae levels T13, T11 and T7 to expose spinal levels L5, L1 and T9. A concentric bipolar stimulating electrode (FHC CBBPC75) was placed over the dorsal columns at L5 for local surface stimulation (stimulation range: 100  $\mu$ sec at 0.1 mA to 0.5 mA, 0.2 Hz). Field potentials were recorded at either L1 (below the injury) or T9 (above the injury) with a fine microneurography electrode (in-house custom made) inserted superficially into the spinal cord. Recordings were filtered between 300 and 6 kHz; amplified by 4 k. The animals were grounded with a 30 G needle through the skin. The traces had a typical positive-negative-positive waveform corresponding to the compound action potential in the dorsal column (50) with a conduction velocity of around 25 msec (51). To capture all components of the compound action potentials, we analysed the area under the curve by measuring the absolute integral of the curves (between 1 and 11 msec). 5 traces were averaged per mouse for analysis and representation at a stimulation intensity that distinctively excites dorsal column fibres controlled for by recording from below the lesion site.

## **Hoffmann-Reflex Testing**

Electrophysiology was performed as previously reported (52). Briefly, rats were anaesthetized with 30 mg/kg ketamine and 0.1 mg/kg medetomidine and two 24-G needle electrodes were inserted across the lateral side of the ankle for nerve stimulation (via a constant current isolated pulse stimulator, stimulus width 100  $\mu$ s). Two recording electrodes were inserted into the medial plantar foot to record electro myograms. The signal was amplified (1000-fold), filtered (10 Hz to 5 kHz), digitized via PowerLab, visualised and analysed with LabChart. The M-wave is evoked by excitation of motor axons. The H-wave is the monosynaptic reflex: Ia

proprioceptive afferents synaptically activate motor neurons in the spinal cord. The threshold was determined as the lowest stimulation intensity that elicited a H-wave response in at least 75% of the recordings. First, the responses to increasing stimulus intensities were tested at 0.1 Hz up to 2 x threshold. M-wave and H-wave amplitudes were normalized to the maximum M-wave recorded at higher stimulation intensities.

### **Laser capture micro-dissection**

Sciatic L4-L6 DRGs were extracted from 3 mice per condition. Using RNase-free conditions, DRGs were embedded with Tissue Freezing Medium (Triangle Biomedical Sciences, Inc) and frozen in dry ice-cold 2-methylbutane. 16  $\mu$ m thick sections were cut on the cryostat and collected on Leica PEN-membrane slides (Leica). From each animal, 4-6 slides were obtained. Toluidine blue (Sigma) staining was used to identify the DRG neurons. Slides containing sections were dehydrated and stained with ethanol series, as follow: 3 times of 30 seconds in 70% ethanol, 60 seconds in 0.5% Toluidine blue dissolved in 70% ethanol, 2 times for 30 seconds each in 70% ethanol, 1 time for 30 seconds in 90% ethanol, 2 times for 30 seconds in 100% ethanol. Once air-dried the slides underwent laser capture using a Leica LMD 6000 microscope. From each animal, large diameter neurons with a diameter of  $\geq 30$  microns were obtained.

### **Western Blot**

Proteins from L4–L6 DRGs were extracted using RIPA buffer with protease and phosphatase inhibitor cocktails (Roche), lysed for 30 min on ice followed by 30 min centrifugation at 4 °C. Protein concentration was quantified using Pierce BCA Protein Assay Kit (ThermoScientific). Subsequently, 10–50  $\mu$ g protein was loaded in SDS–polyacrylamide gel electrophoresis (PAGE) gels and transferred to polyvinylidene difluoride (PVDF) membranes for 2 h. Membranes were blocked with 5% BSA or milk for 1 h at room temperature and then incubated with H4K8ac (1:1000, ab15823), H4 (1:1000, Abcam ab10158), CREB (1:500, Abcam ab178322), pCREB (1:500, Abcam ab32096) or GAPDH (1:1000, cell signaling 14C10) antibodies at 4 °C overnight. Membranes were then incubated with HRP-linked secondary antibody (GE Healthcare) for 1 h at room temperature and developed with ECL substrate.

### **RNA sequencing**

RNA sequencing was performed using RNA from whole DRG tissue and from large diameter laser microdissected DRG neurons in 3 biological replicates. For whole DRG RNAseq, sciatic L4-L6 DRGs were extracted from 2 mice per sample and stored in RNase later (Qiagen). DRG tissue was crushed with RNase free micropestle and RNA was extracted using RNeasy kit (Qiagen), according to manufacturer's protocol. Residual DNA contamination was removed by on column DNase I treatment (Qiagen) for 15 min at room temperature. RNA concentrations and quality were measured using Agilent 2100 Bioanalyzer (Agilent). RNA with RIN factor above 7.5 was used for library preparation. Libraries were prepared at Ospedale San Raffaele (Milan) using the TruSeq mRNA Sample Preparation kit (Illumina) and sequenced using Illumina HiSeq 2500 100-cycle, pair end sequencing.

For Laser captured DRG neurons, RNA was extracted using Arcturus PicoPure RNA isolation kit (Life Technologies), following manufacturers protocol. RNA concentrations and quality were measured using Agilent 2100 Bioanalyzer (Agilent). RNA with RIN factor between 6 and 7 were used for library preparation. Libraries were prepared using the RiboZero ScriptSeq V2 kit working from the low input protocol using 100 ng of RNA per sample. Libraries were sequenced using Illumina HiSeq 2500 generating 125 bp, paired end reads. Sequence reads were aligned to the mm10 mouse reference genome sequence using tophat version 2.0.12 running Bowtie2-2.2.3. Gene structure annotations corresponding to the Ensembl annotation of the mm10 genome sequence were used to build a transcriptome index

and provided to tophat during the alignment step. The aligned reads were sorted using samtools-0.1.19 and read counts per gene were obtained from mapped reads using HTSeq-0.6.1. EdgeR version 3.8.6 (using limma-3.22.7) in R-3.1.1 was used to identify differentially expressed genes. Read-level quality checking was performed using fastqc-0.10.1 and the fastqc-aggregator ([https://github.com/staciaw/fastqc\\_aggregator](https://github.com/staciaw/fastqc_aggregator)) and gene-level quality checking was performed using RSeQC-2.6.1. The gene expression in EE was compared to SH. Heatmap of RNAseq mRNA expression levels of the genes differentially expressed in any sample group ( $P < 0.05$ ) was generated using Euclidean unsupervised hierarchical clustering in Matlab R2014b using the custergram function.

Gene ontology (GO) and KEGG (Kyoto Encyclopedia of Genes and Genomes) were performed on the differentially expressed genes with DAVID (Database for Annotation, Visualization, and Integrated Discovery (<http://david.abcc.ncifcrf.gov/>)) using a threshold of  $P < 0.05$ . Functional GO clustering was performed using ClueGO in Cytoscape (<http://www.cytoscape.org/>): (Bonferroni  $P \leq 0.05$ ) (GO tree interval min3, max8) (GO selection min 4, 1%) (K score 0.3). Differentially expressed proteins and genes that resulted enriched in the GO functional clustering were uploaded into STRING to build a protein-protein interaction network. The network was visualized by Cytoscape, where each node represents a differentially regulated gene (RNA-seq) or protein (proteomic) and edges represent protein-protein interactions.

### **Axoplasm extraction and proteomics**

Sciatic nerves were dissected and the axoplasm was obtained according to the previously published protocol (53). LC-MS was performed on axoplasmic samples by the Quantitative Biology Center (QBiC) in Tuebingen followed by proteomics analysis. Each axoplasmic extract processed for proteomics was derived by pooling 16 nerves dissected from 8 mice that were housed for 10 days in either SH or EE in biological triplicates and technical duplicates. The raw data was processed with MaxQuant version 1.5.0.25. The protein and peptides intensities were normalized using the "quantile normalization" procedure in R. The differential expression analysis of the proteins and peptide modifications was performed by the means of mixed linear models R (nlme) and ANOVA. The effect of treatment (SH vs EE) on protein expression was modelled as: intensity ~ treatment, with technical replicates nested within biological replicates as random factor. Correction for multiple hypothesis testing was done by R (qvalue) at  $FDR < 0.05$ .

### **Ca imaging**

PV-cre x GCaMP mice were housed in EE or SH for 10 days. L4-L6 DRGs were extracted and immediately suspended in HBBS without  $Ca^{2+}$  (Thermofisher) with 10 mM Hepes (Thermofisher) at 37°C, 5%  $CO_2$ . The DRGs were then placed into a video-microscopy chamber at 37°C and suspended in HBBS without  $Ca^{2+}$  (Thermofisher), to avoid any calcium influx from extracellular medium. Time-lapse recordings were taken with images acquired every 1 second for 5 minutes. Imaging was done on a Nikon Eclipse TE2000 microscope with a optiMOS scMOS camera using 20X magnification. After 30 seconds of baseline recording, increasing concentrations (50 mM, 100 mM and 150mM) of KCL (Sigma) were added to the DRG to elicit depolarisation and induce intracellular  $Ca^{2+}$  release. Quantification was done using the ImageJ plug-in *Time series analyser*, where the soma of all PV neurons were analysed per DRG, 6 DRG's per mouse and 4 mice per condition. To determine the fold-change in GCaMP intensity after KCL addition, the GCaMP intensity ratio "F/Fo" was calculated by dividing the average fluorescence intensity after KCL addition "F" with the average intensity of baseline fluorescence "Fo".

### **Cytokine Assay**

Sciatic L4-L6 DRGs (pool of 4 mice) and serum (pool of 2-4 mice) were collected in 3 biological replicates. 100 µl of serum (corresponding to 1.5 mg of proteins) was run on a Mouse Cytokine Array Panel A (R&D System) and developed according to manufacturer's protocol to quantify cytokine levels. The resulting spots on the membrane were quantified by densitometry and the signal intensity in the EE samples was referred to the SH control.

### **Neurotrophin ELISA**

Levels of neurotrophins were analysed in homogenised L4-6 DRG samples and blood serum. Blood serum was diluted 1:7 to avoid matrix interference, while DRGs were lysed in RIPA buffer and diluted 1:6. 100 µl of serum (corresponding to 0.2 mg of proteins) and 100 µl of lysate (corresponding to 80 mg of proteins) were analysed with the Multi-Neurotrophin Rapid Screening ELISA kit (Biosensis), according to manufacturer's instructions. The absorbance at 450 nm of the samples, obtained using GLoMax plate reader (Promega), was interpolated against the standard curve to calculate the neurotrophin concentration, and referred to mg of proteins.

### **Synthesis of carbon nanospheres of average size 350nm**

5 g of D(+) glucose was dissolved in 50 mL of deionised water to form a clear solution. The solution was placed in a 65 mL teflon lined sealed stainless steel autoclave and maintained at 180 °C for 12 hr. The products were centrifuged at 10000 rpm for 10 min and were washed with water and ethanol thrice each before being dried in the oven at 60 °C for 4 hr. The final product is a brownish powder which had spheres with an average size of 350 nm.

### **Synthesis of TTK21**

To the Dichloromethane (DCM) solution of 2-Propoxy Benzoic Acid (3.3mmol) one equivalent of thionyl chloride (3.66 mmol) and 4-5 drops of N, N-Dimethylformamide (DMF) were added and the solution was refluxed for 4hr. Thionyl chloride was removed by evaporating the solvent 3-4 times and to that DCM was added (Solution A). To the DCM solution of 4-Chloro-3-(trifluoromethyl) amine (3.1 mmol) a few drops of triethylamine was added at 0 °C and was stirred for 30 min (Solution B). The solution B was added drop-wise to the solution A at 0 °C and after sometime the solution was heated to reflux for 4 hr. Then the solution was evaporated to dryness and was purified by column chromatography. White crystalline solid was obtained.

### **Conjugation of TTK21 to CSP**

CSP suspension in DCM was reacted with one equivalent of SOCl<sub>2</sub> and few drops of DMF. The reaction mixture was refluxed at room temperature for 4hr. Thionyl chloride was removed by evaporating the solvent 3-4 times and to that DCM was added to make the suspension. To that suspension one equivalent TTK21 and few drops of triethylamine were added. The reaction was refluxed for 4 hr. The suspension was filtered and the precipitate was washed with DCM. The conjugated CSP-TTK21 was dried. The conjugation of TTK21 to the nanosphere was analysed by Energy Dispersive X-ray Spectroscopy EDX. The spectrum of CSP-TTK21 shows that wt % of Fluorine is 0.31 which belongs to TTK21 indicating the covalent conjugation of TTK21 to CSP.

### **CSP-TTK21 administration**

Animals were randomised to treatment with the CBP/p300 activator bound to carbon nanospheres (CSP-TTK21) or a control of just carbon nanospheres (CSP) (mice – 20 mg/kg, rats – 10 mg/kg injected IP once a week). Mice received the first IP injection 4 hours after SCI and rats received the first IP injection 6 hours after SCI to simulate a clinically-feasible delay-to-treatment and then once a week thereafter. The optimal dose and time-course for retention of the small molecule-bound nanospheres in the CNS had been previously determined (33). CSP-TTK21 activates CBP 4 fold more potently than p300. No adverse effects were observed

following IP administration of CSP-TTK21 and after histological analysis no obvious cellular toxicity was observed.

### AAV-DREADD experiments

Non-Cre dependent DREADD AAV vectors (AAV5-CaMKIIa-EGFP, AAV-CaMKIIa-HA-hM3D(Gq)-IRES-mCitrine, AAV-CaMKIIa-HA-hM4D(Gi)-IRES-mCitrine) were purchased from UNC vector core. Viral titres were matched to  $1 \times 10^{13}$  GC/ml. 3  $\mu$ l of Non-cre dependent AAV vector was injected in to the sciatic nerve to transduce DRG neurons. 4 weeks later the mice were placed in EE or SH for 10 days and given 0.05 mg/ml CNO with 5 mM sucrose in their drinking water each day, mice received approximately 5mg/kg CNO per day.

To determine whether any observed increase in conduction across the lesion site was contingent on regenerating axons. Cre-dependent AAV-DREADD vector (AAV-hSyn-DIO-hM4D(Gi)-mCherry) was purchased from UNC vector core. Titre was  $1 \times 10^{13}$  GC/ml. 3 weeks after a T9 dorsal hemisection 0.5  $\mu$ l of cre-dependent AAV5-DREADD-Gi vector was injected in to the spinal cord at T7. 3 weeks later during terminal electrophysiological experiments mice received an I.P. injection of CNO (1.2 mg/kg body weight).

### Statistical analysis

Results are expressed as mean values  $\pm$  SEM and n values represent the number of animals in the experiment. Statistical analysis was carried out using Graphpad Prism 7 (GraphPad, prism software). The Kolmogorov–Smirnov and Levene’s tests were used to test for normality and the equality of variances. A two-tailed unpaired Student’s *t*-test, one-way ANOVA for evaluation of experiments with more than two groups, and one- or two-way repeated-measures ANOVA for functional assessments, were used. Tukey’s, Sidak’s or Fisher’s LSD post-hoc tests were applied when appropriate. Behavioral assays were replicated two or three times, depending on the experiment, and averaged per animal. Statistics were then performed over the mean of animals. A threshold level of significance  $\alpha$  was set at  $P < 0.05$ . Significance levels were defined as follows: \* $p < 0.05$ ; \*\* $p < 0.01$ ; \*\*\* $p < 0.001$ .

### Supplementary Figures

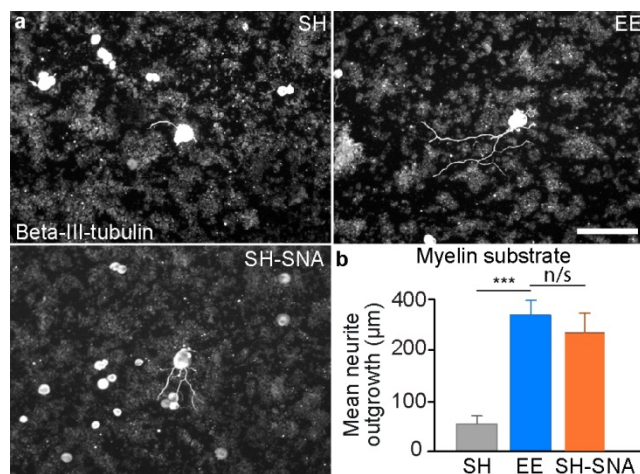


**Fig. S1 Exposure to EE enhances neurite outgrowth on inhibitory myelin substrate to a similar extent as a conditioning SNA injury. (A)** Representative images of DRG neurons cultured on an inhibitory myelin substrate for 12 hours and stained for Beta-III-tubulin. Scale



bar, 100  $\mu\text{m}$ . **(B)** Quantification of neurite outgrowth per neuron demonstrated that EE significantly increased neurite outgrowth compared to SH to a similar level as SNA (mean  $\pm$  SEM, One-way ANOVA, Tukey's post-hoc \*\*\*  $P < 0.001$ ,  $n = 4/\text{group}$ ).

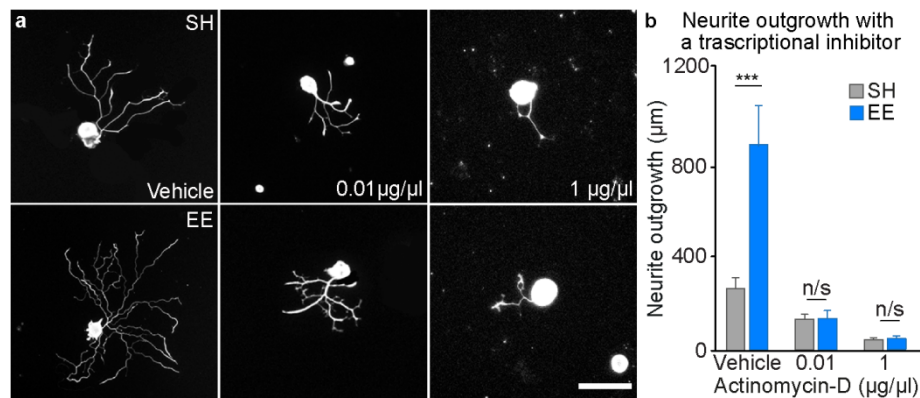


**Fig. S2 Inhibiting transcription with actinomycin-D blocks the EE-mediated increase in DRG neurite outgrowth.** (A) Representative images of DRG neurons cultured for 12hr with vehicle, 0.01  $\mu\text{g}/\mu\text{l}$  or 1  $\mu\text{g}/\mu\text{l}$  actinomycin-D. (B) Quantification of neurite outgrowth per neuron demonstrated that the EE-mediated increase in neurite outgrowth was dependent on active transcription (mean  $\pm$  SEM, One-way ANOVA, Tukey's post-hoc,  $n = 4/\text{group}$ ).

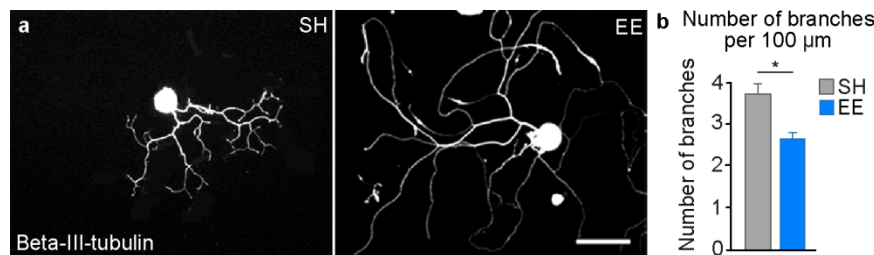


**Fig. S3. Exposure to EE enhances axon elongation rather than branching.** (A) Representative images of cultured DRGs from mice that had been in SH or EE for 10 days, DRGs were stained for Beta-III-tubulin. Scale bar, 100  $\mu\text{m}$ . (B) Quantification of the mean number of branches per 100  $\mu\text{m}$  showed a significant reduction in neurite branching after exposure to EE (mean  $\pm$  SEM, unpaired Student's t test \*  $P < 0.05$ ,  $n = 4/\text{group}$ ).

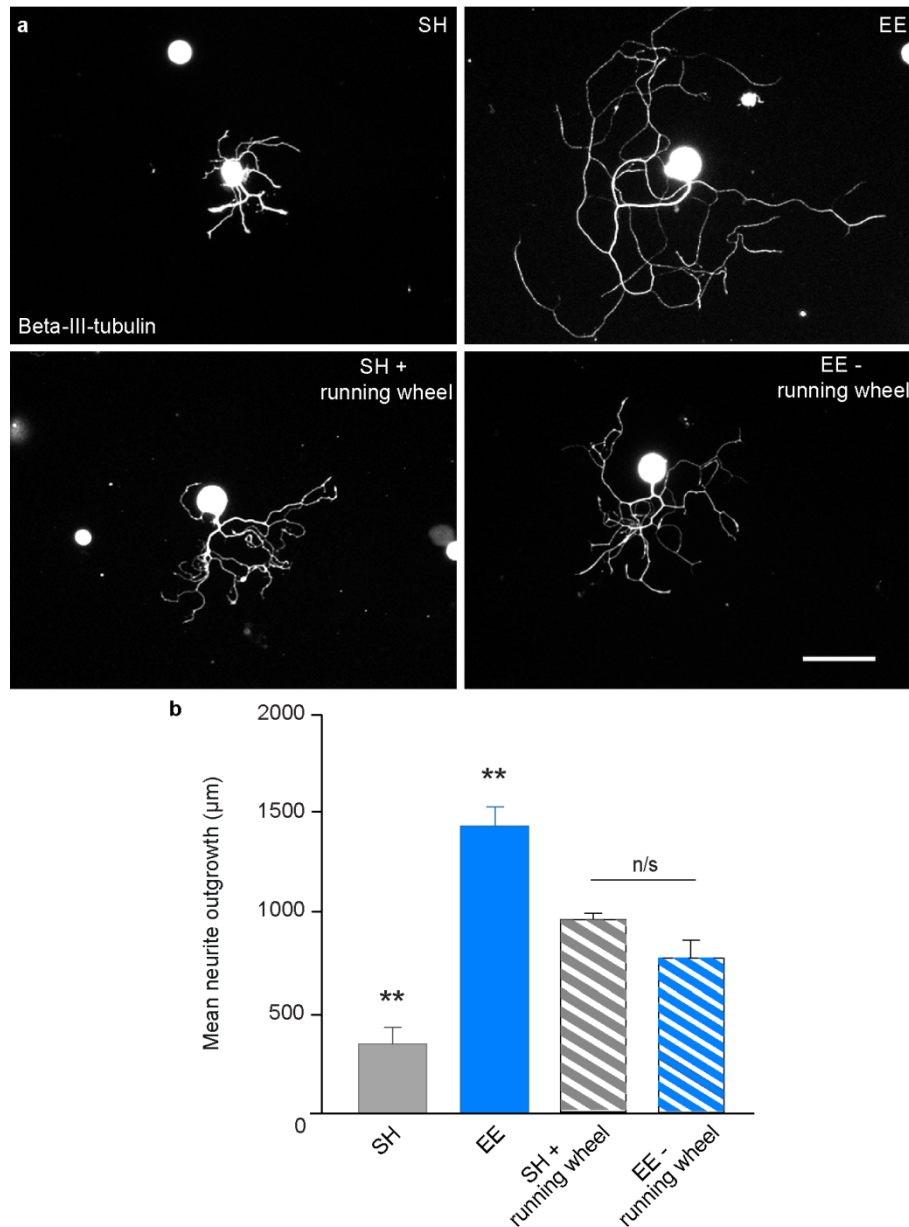


**Fig. S4. The full EE increases DRG neurite outgrowth compared to the running wheel alone.** (A) Example images of cultured DRGs stained for Beta-III-tubulin after exposure to EE, SH, SH with a wheel or EE with an immobilised wheel. Scale bar, 100 μm. (B) Mean neurite outgrowth per neuron was quantified and we observed a significant difference between all the groups except the SH + wheel and EE – wheel groups (mean ± SEM, One-way ANOVA, Tukey's post-hoc \*\*  $P < 0.01$ ,  $n = 4/\text{group}$ ).



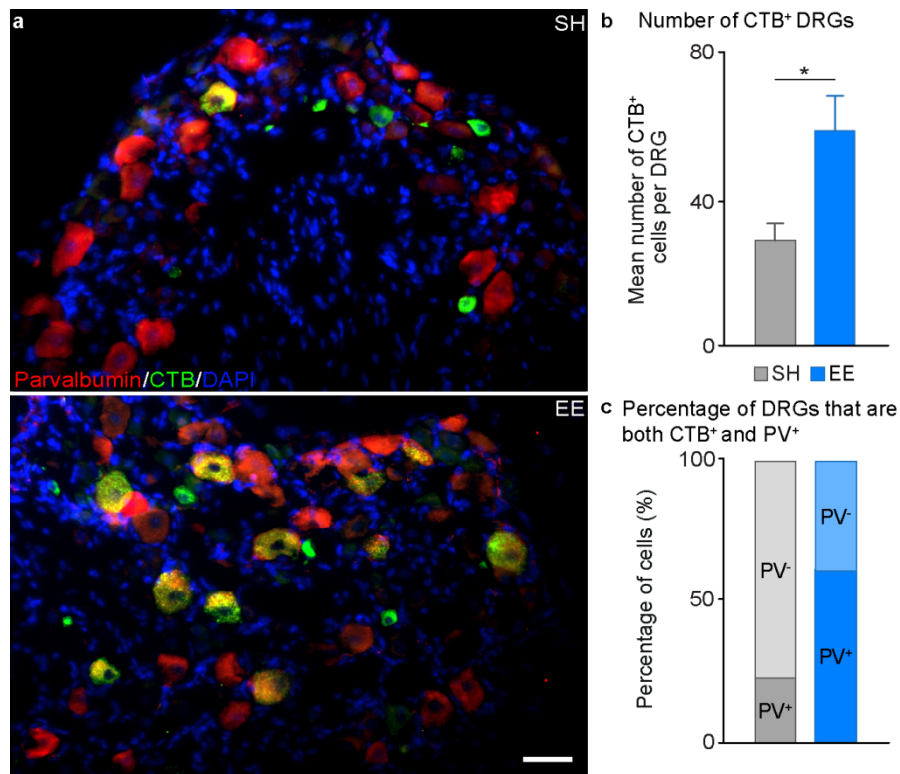


**Fig. S5. Exposure to EE enhances muscle re-innervation by proprioceptive DRG neurons.** (A) Representative images of sciatic DRGs from mice that had been in SH or EE for 10 days prior to a sciatic nerve crush injury, followed by injections of CTB into hind limb muscles 14 days later to assess muscle re-innervation. (B) Quantification of the number of CTB positive DRG neurons suggests EE significantly enhances muscle re-innervation compared to SH (mean  $\pm$  SEM, unpaired Student's t test, \*\*  $P < 0.01$ ,  $n = 4$ /group). (C) Quantification of the percentage of CTB positive neurons that co-localized with parvalbumin demonstrates a higher level of co-localization between CTB and parvalbumin after exposure to EE.

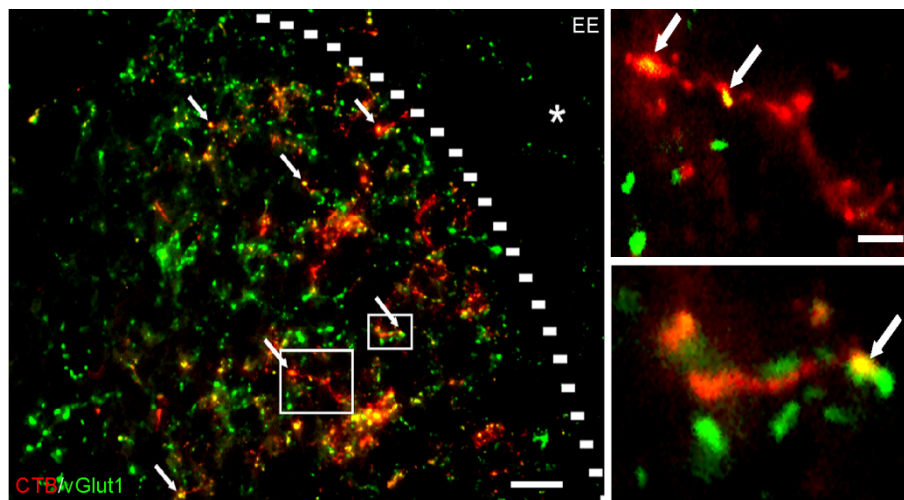
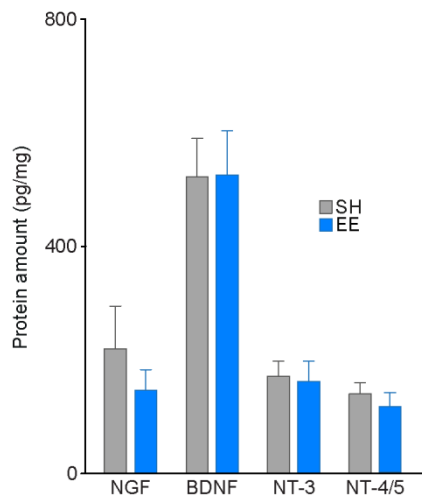


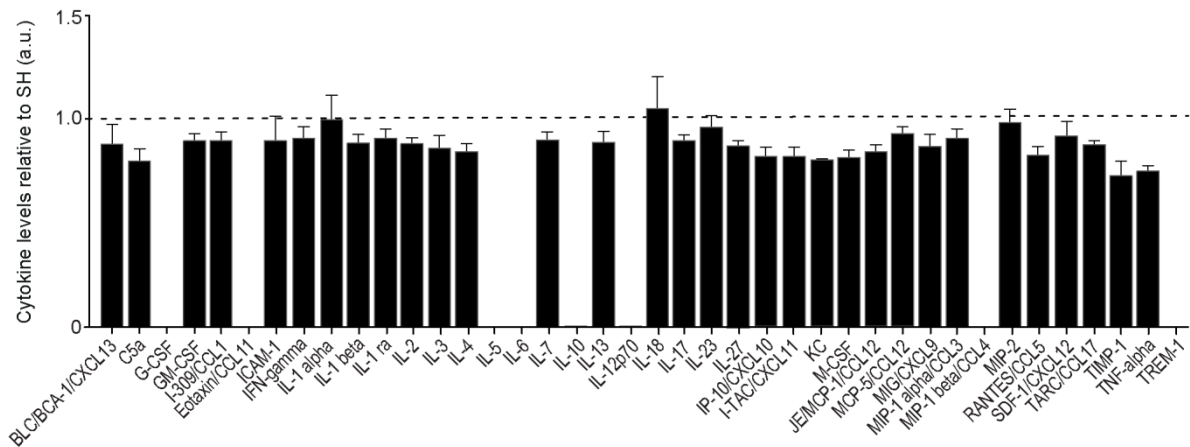
**Fig. S6. EE promotes axon regeneration and the formation of putative synapses.** Representative image from a EE mouse showing co-localisation of regenerating CTB (red) positive axons rostral to the spinal cord injury site (marked by the dashed line and asteriks) with the pre-synaptic marker vGlut1 (green) to identify presynaptic excitatory boutons and prospective nascent synapses (marked by arrows). Scale bar, 100  $\mu$ m. Higher-magnification

images of insets in show co-localisation of CTB positive axons (red) and vGlut1 (green). Scale bar, 10  $\mu$ m.

**a** Neurotrophin levels in the whole DRG



**b** Cytokine levels in DRG



**c** Cytokine levels in blood serum

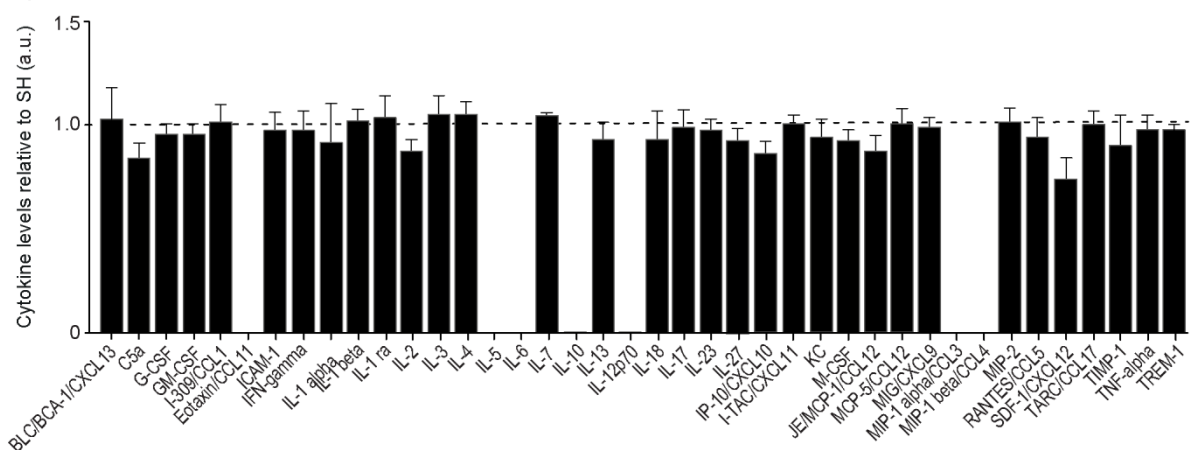


**Fig. S7. Neurotrophin and cytokine levels in the DRG and blood serum are not affected by EE.** (A) Quantification of neurotrophin protein levels in whole DRG lysate shows no significant differences between SH and EE (mean  $\pm$  SEM, Two-way ANOVA, Sidak's post-hoc,  $n = 3$ /group). (B) Quantification of cytokine levels in whole DRG lysate shows no differences between SH and EE (mean  $\pm$  SEM, Two-way ANOVA, Sidak's post-hoc,  $n =$

4/group). (C) Quantification of cytokine level in blood serum shows no differences between SH and EE groups (mean  $\pm$  SEM, Two-way ANOVA, Sidak's post-hoc, n = 4/group).

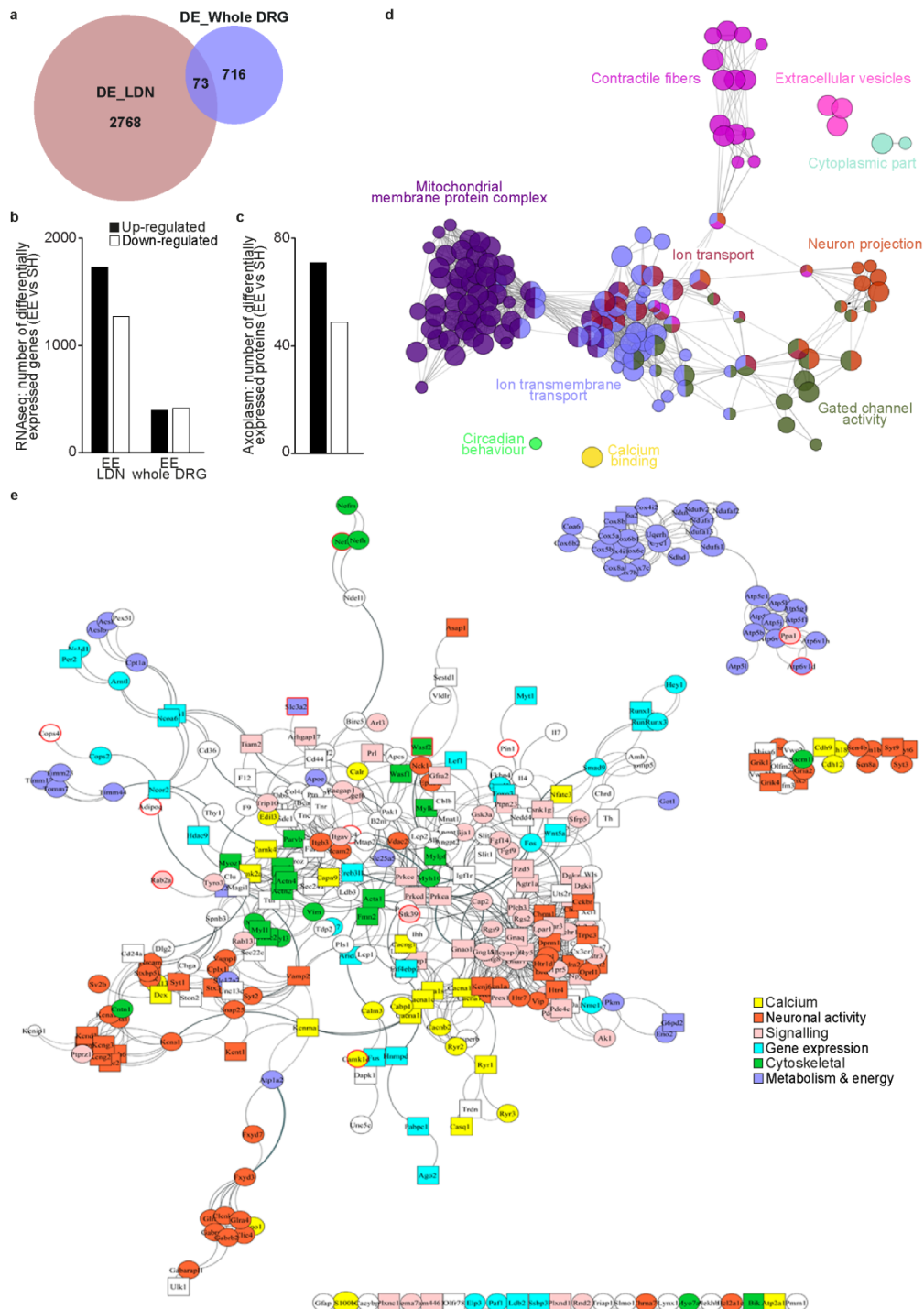


**Fig. S8. RNAseq and proteomic datasets demonstrate that EE strongly modulates pathways involved in neuronal activity, calcium signaling, gene expression and cytoskeletal changes. (A)** Area proportional Venn diagram of differentially expressed (DE) genes ( $P < 0.05$ ) in Whole DRG vs LDN. **(B)** Histogram of the numbers of DE genes ( $P < 0.05$ ) in the Whole DRG vs LDN and **(C)** axoplasmic proteins ( $P < 0.05$ , or difference  $\geq 4$  peptides). **(D)** GO clustering of the DE genes in LDN dataset run with ClueGO in Cytoscape: (Bonferroni

$P \leq 0.05$ ). Each edge represents interrelation between terms, defined by the K score. **(E)** Cytoscape visualization of the protein-protein interactions calculated by String. Each node represents a DE gene (RNAseq) or protein (proteomic). Red borders highlight nodes found DE at both gene and protein level. Edges represent protein-protein interactions, where their width reflects the Edge Betweenness. Circle shape: Up-regulated. Square shape: down-regulated. The size of the node reflects the Betweenness Centrality. Functional groups are highlighted in different colors.

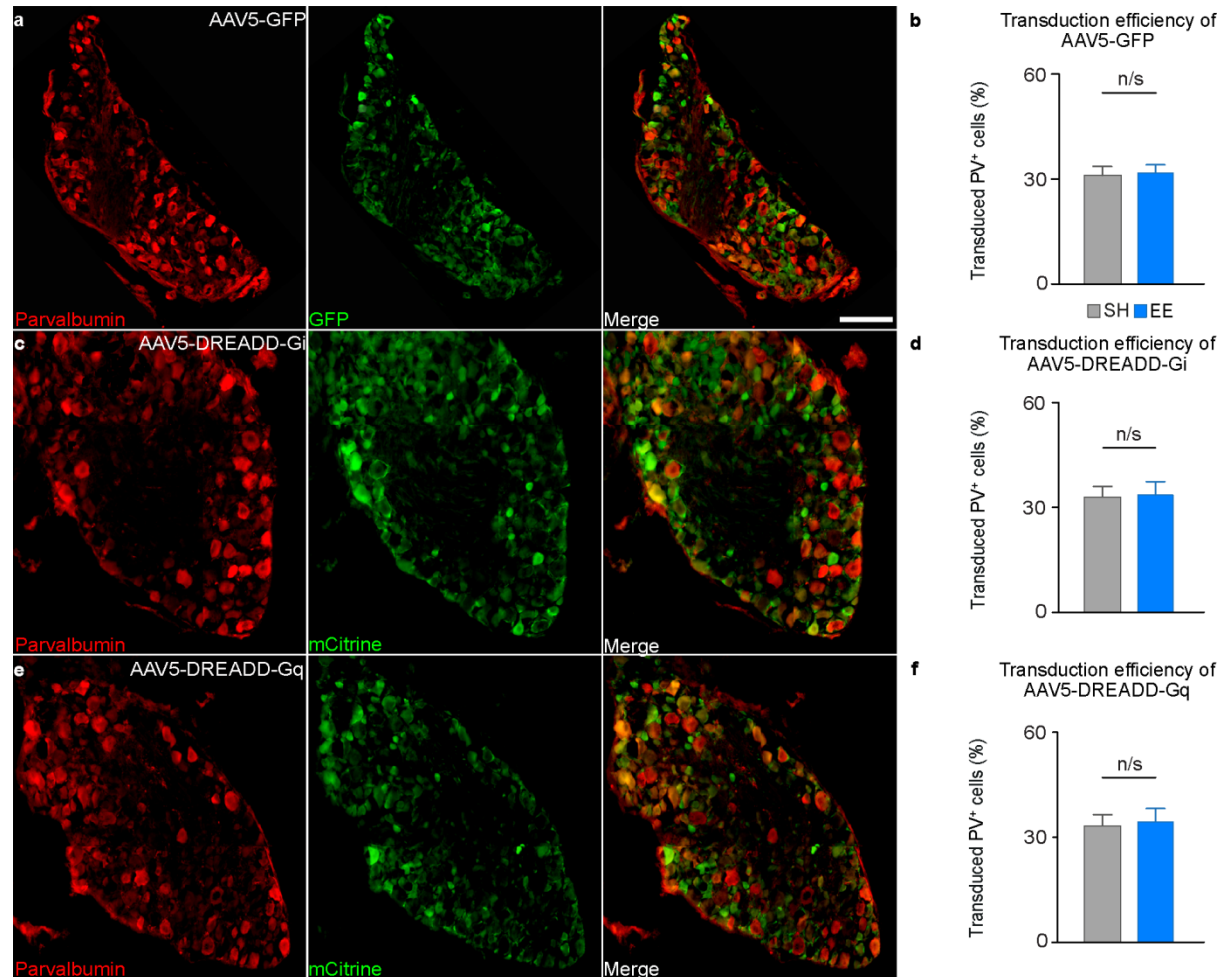


**Fig. S9. Efficient transduction and DREADD expression in parvalbumin positive DRGs.** **(A)** Image of a DRG section transduced with AAV5-GFP (green) and stained with parvalbumin (red). Scale bar, 50  $\mu$ m. **(B)** Quantification of transduction efficiencies of AAV5-GFP in parvalbumin positive DRGs (mean  $\pm$  SEM, unpaired Student's t test n/s, n = 6/group). **(C)** Image of a DRG section transduced with AAV5-hM4Di-mCitrine (green) and stained with parvalbumin (red). Scale bar, 50  $\mu$ m. **(D)** Quantification of transduction efficiencies of AAV5-hM4Di-mCitrine in parvalbumin positive DRGs (mean  $\pm$  SEM, unpaired Student's t test n/s, n = 6/group). **(E)** Image of a DRG section transduced with AAV5-hM3Dq-mCitrine (green) and stained with parvalbumin (red). Scale bar, 50  $\mu$ m. **(F)** Quantification of transduction efficiencies of AAV5-hM3Dq-mCitrine in parvalbumin positive DRGs (mean  $\pm$  SEM, unpaired Student's t test n/s, n = 6/group).

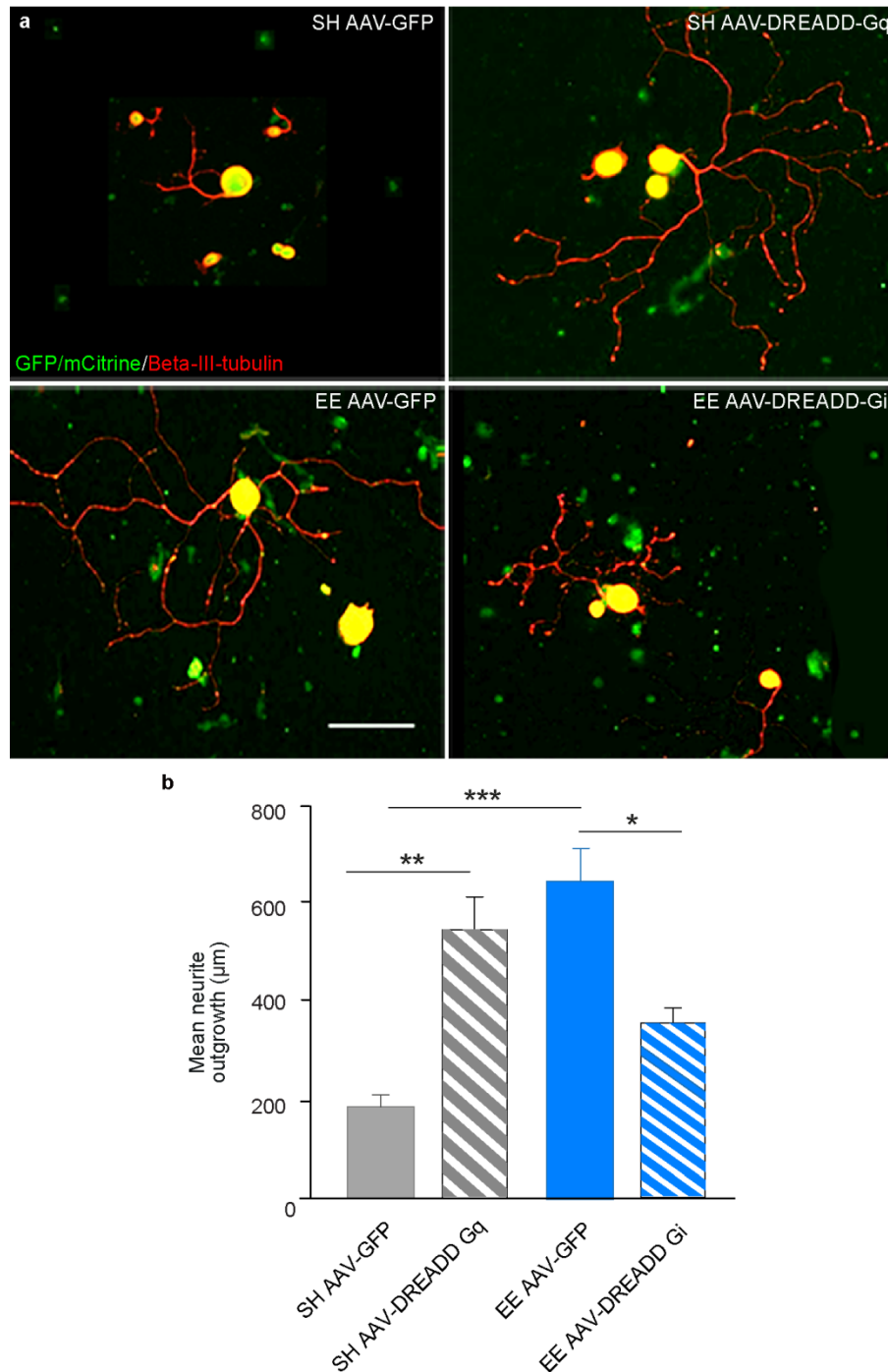


**Fig. S10. The EE-mediated increase in DRG neurite outgrowth is mediated by neuronal activity.** (A) Example images of cultured DRGs which had been transduced with AAV-GFP, AAV-DREADD-Gi or AAV-DREADD-Gq and then exposed to SH or EE for 10 days. AAV vectors expressed GFP or mCitrine (green) to identify transduced DRGs which were also stained for Beta-III-tubulin (red). Scale bar, 100  $\mu\text{m}$ . (B) Quantification of the neurite outgrowth per neuron showed that increasing neuronal activity with DREADD-Gq in DRGs from SH mice increased outgrowth to a similar level as EE. Silencing DRGs from EE mice with DREADD-Di significantly reduced neurite outgrowth compared to EE (mean  $\pm$  SEM, One-way ANOVA, Tukey's post-hoc \*  $P < 0.05$ , \*\*  $P < 0.01$ , \*\*\*  $P < 0.001$ ,  $n = 4/\text{group}$ ).



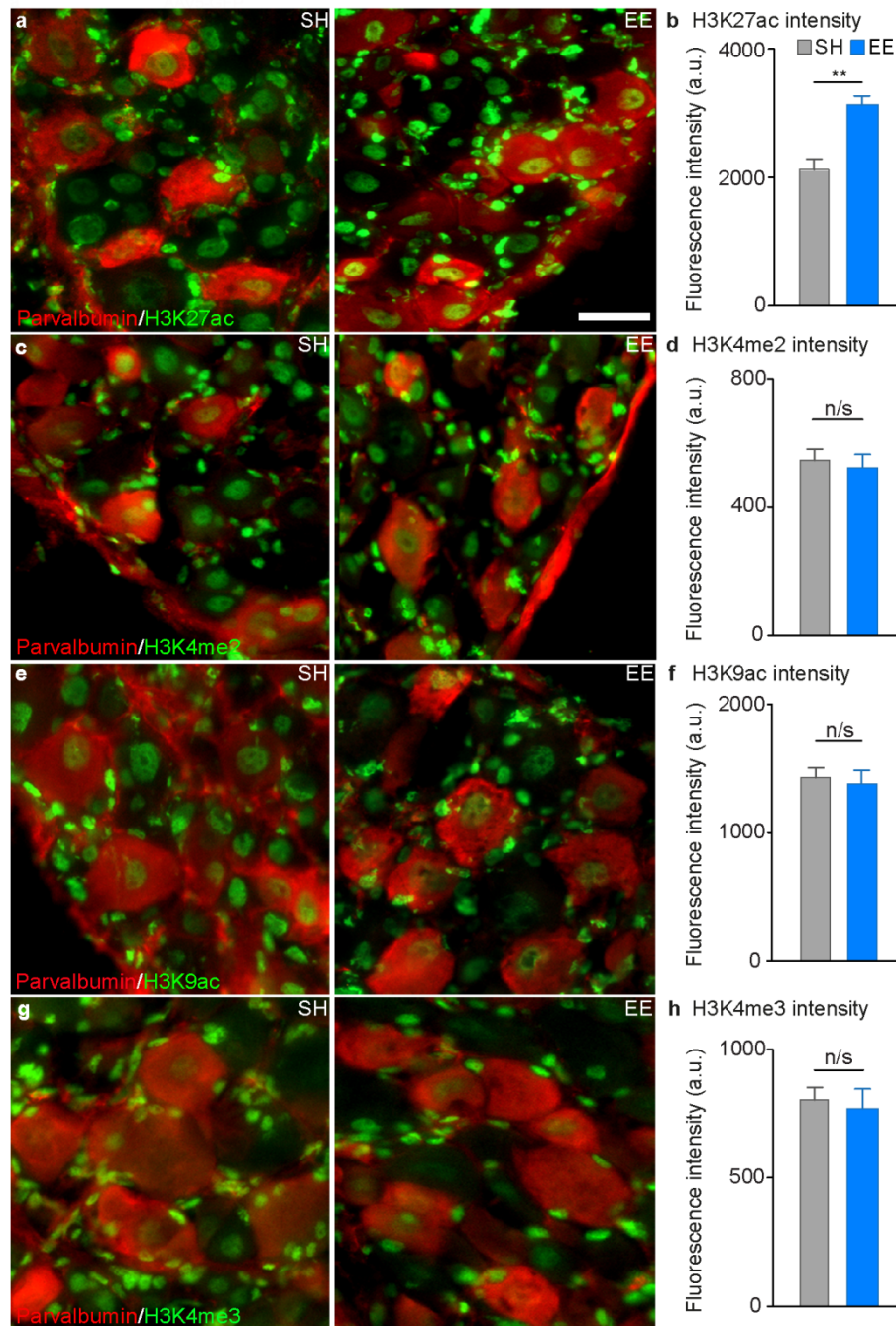


**Fig. S11. H3K27ac is increased in parvalbumin positive DRGs after exposure to EE but the levels of H3K4me2, H3K9ac and H3K4me3 do not change compared to SH. (A)** Representative images of DRGs from mice housed in SH or EE, which were stained for H3K27ac (green), parvalbumin (red). Scale bar, 50  $\mu$ m. **(B)** Quantification of the fluorescence intensity of H3K27ac in the nuclei of parvalbumin positive DRGs showed a significant increase after EE compared to SH (mean  $\pm$  SEM, unpaired Student's t test \*\*  $P < 0.01$ ,  $n = 4$ /group). **(C, E and G)** Representative images of DRG from mice that had been exposed to SH or EE for 10 days and then stained for parvalbumin (red) and H3K4me2 **(C)** H3K9ac **(E)** and H3K4me3 **(G)** in green. Scale bar, 50  $\mu$ m. **(D, F and H)** Quantification of the fluorescence intensity of H3K4me2, H3K9ac and H3K4me3 in the nuclei of parvalbumin positive DRGs showed no significant difference between the SH and EE groups (mean  $\pm$  SEM, unpaired Student's t test,  $n = 4$ /group).

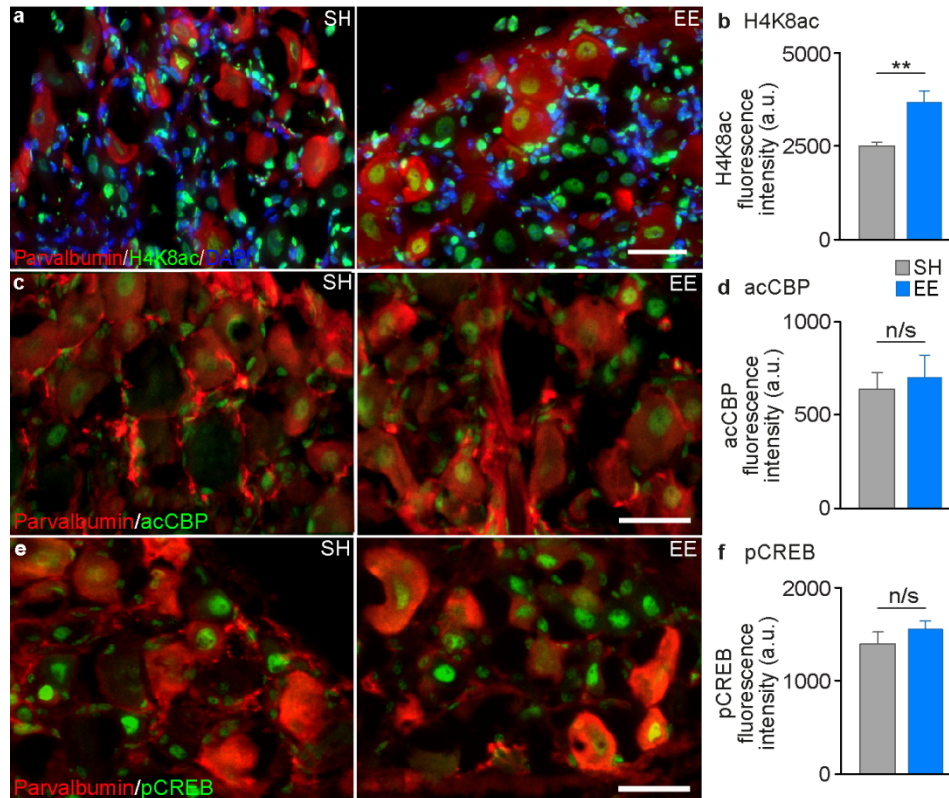


**Fig. S12. Levels of H4K8ac but not acCBP or pCREB remain elevated in parvalbumin positive DRGs for 5 weeks after exposure to EE.** (A) Images of DRGs stained for parvalbumin (red) and H4K8ac (green) and DAPI (blue) from mice exposed to SH or EE for 10 days and then placed in SH for 5 weeks. Scale bar, 50  $\mu$ m. (B) Quantification of the fluorescence intensity of H4K8ac demonstrated a significant increase in parvalbumin positive DRGs from mice previously exposed to EE compared to SH (mean  $\pm$  SEM, unpaired Student's t test \*\*  $P < 0.01$ ,  $n = 6$ /group). (C) Images of DRGs stained for parvalbumin (red) and acCBP (green) from mice exposed to SH or EE for 10 days and then placed in SH for 5 weeks. Scale bar, 50  $\mu$ m. (D) Quantification demonstrated no significant increase in acCBP levels in parvalbumin positive DRGs from mice previously exposed to EE (mean  $\pm$  SEM, unpaired Student's t test, n/s,  $n = 6$ /group). (E) DRGs stained for parvalbumin (red) and pCREB (green) from mice exposed to SH or EE for 10 days and then placed in SH for 5 weeks. Scale bar, 50  $\mu$ m. (F) Quantification showed no significant increase in pCREB levels in parvalbumin positive DRGs from mice previously exposed to EE (mean  $\pm$  SEM, unpaired Student's t test, n/s,  $n = 6$ /group).

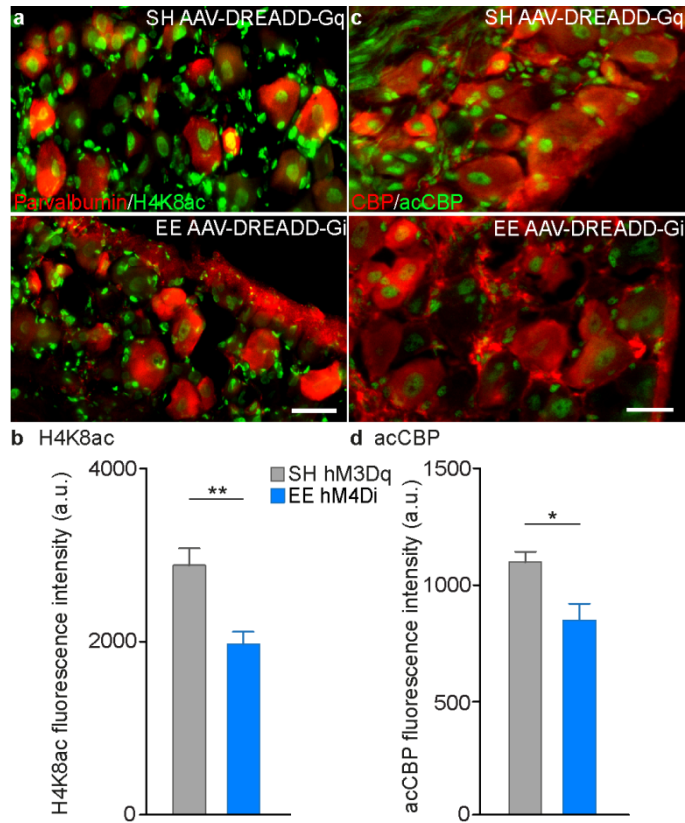


**Fig. S13. Increasing neuronal activity augments the level of H4K8ac and acCBP in DRG neurons.** (A) Images of DRGs stained for parvalbumin (red) and H4K8ac (green) from SH mice expressing hM3Dq or EE mice expressing hM4Di. Scale bar, 50  $\mu$ m. (B) Quantification of the fluorescence intensity of H4K8ac demonstrated a significant increase in parvalbumin positive DRGs from SH mice that express DREADD-Gq compared to DRGs from EE mice that express DREADD-Gi (mean  $\pm$  SEM, unpaired Student's t test \*\*  $P < 0.01$ ,  $n = 6$ /group). (C) Images of DRGs stained for total-CBP (red) and acCBP (green) from SH mice expressing DREADD-Gq or EE mice expressing DREADD-Gi. Scale bar, 50  $\mu$ m. (D) Quantification of the fluorescence intensity revealed that DRGs from SH mice that express DREADD-Gq had significantly increased the levels of acCBP relative to total-CBP compared to DRGs from EE mice that DREADD-Gi (mean  $\pm$  SEM, unpaired Student's t test \*  $P < 0.05$ ,  $n = 12$ /group).



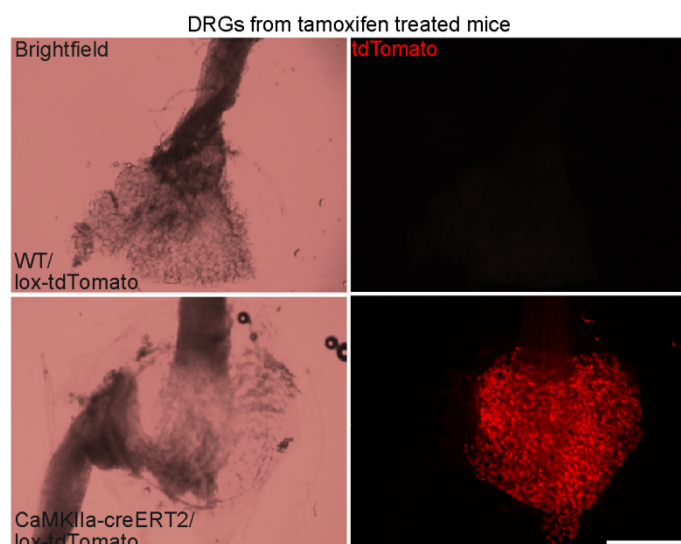


**Fig. S14. The CaMKIIa promoter is active in DRG neurons and drives strong expression of tdTomato after tamoxifen treatment.** Cre-dependent LoxP-STOP-LoxP tdTomato reporter mice were crossed with WT mice or CamKIIa-CreERT2 mice. Tamoxifen treated WT/lox-tdTomato mice show no tdTomato expression in the DRGs. Tamoxifen treated CamKIIa-CreERT2/lox-tdTomato mice show strong expression of tdTomato in DRG neurons. Scale bar, 500  $\mu$ m.

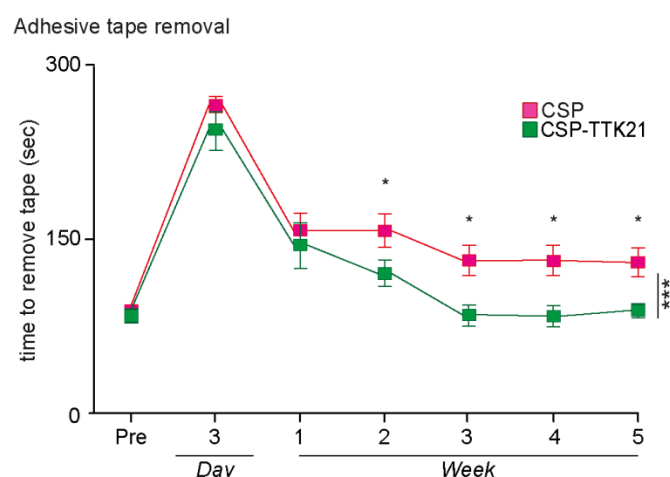


**Fig. S15. CSP-TTK21 treatment significantly enhances the time to remove adhesive tape placed on the hindpaw.** Quantification of the time it took to remove adhesive pad placed on the hindpaws (mean  $\pm$  SEM, Two-way repeated measures ANOVA, Fisher's LSD post-hoc \*\*\* $P$ <0.001, \* $P$ <0.05,  $n$  = 8/group).

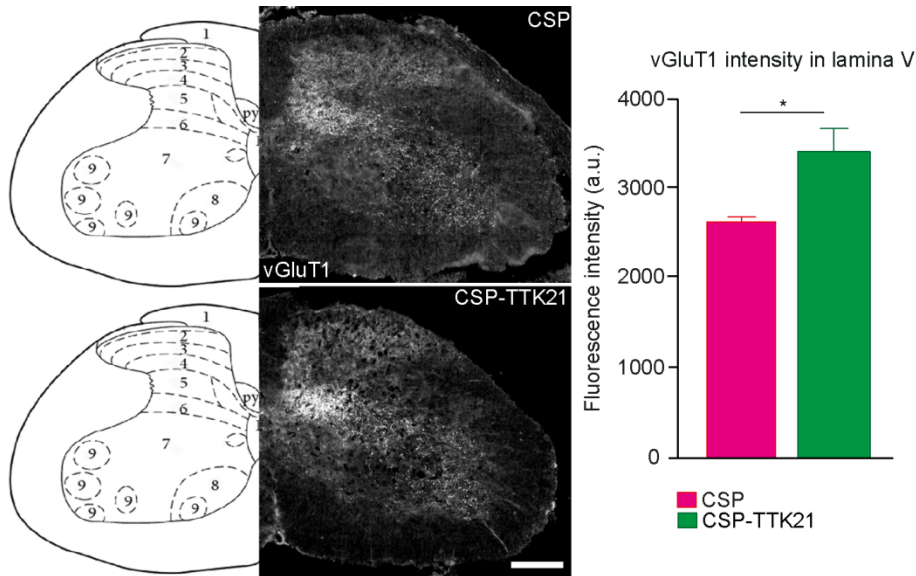


**Fig. S16. CSP-TTK21 treatment promotes sprouting of afferent fibres below the level of injury.** (A) Representative images of one half of the L1-3 spinal cord immunolabelled for vGluT1 from CSP and CSP-TTK21 treated mice, combined to a schematic showing the spinal laminae. Scale bar, 250 µm. (B) Quantification of vGluT1 pixel intensity in lamina V was significantly increased after CSP-TTK21 treatment compared to CSP treatment (mean ± SEM, unpaired Student's t test \*  $P < 0.05$ ,  $n = 8/\text{group}$ ).

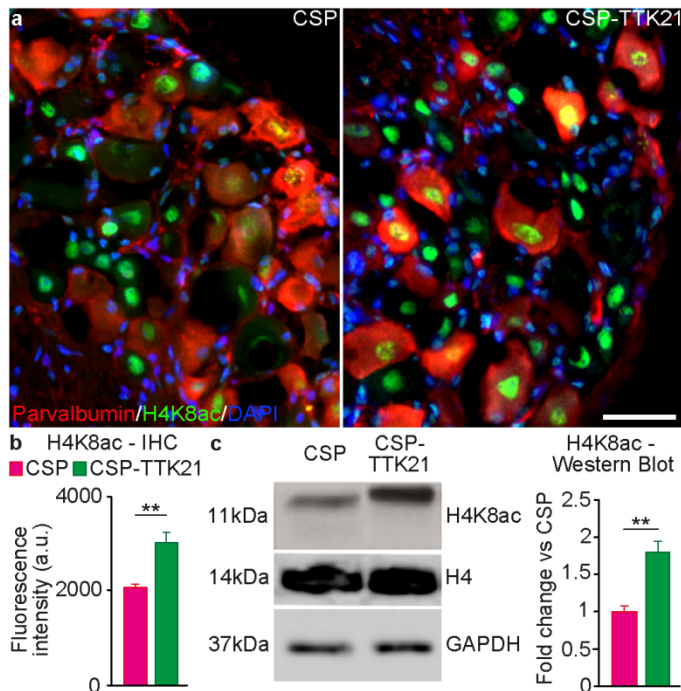


**Fig. S17. CSP-TTK21 treatment enhances H4K8ac in the DRG.** (A) Representative images of DRGs from mice treated with CSP or CSP-TTK21 for 5 weeks, which were stained for H4K8ac (green), parvalbumin (red) and DAPI (blue). Scale bar, 50 µm. (B) Quantification of the fluorescence intensity of H4K8ac in the nuclei of parvalbumin positive DRGs showed a significant increase after CSP-TTK21 treatment compared to CSP (mean ± SEM, unpaired Student's t test \*\*  $P < 0.01$ ,  $n = 4/\text{group}$ ). (C) Immunoblotting analysis for H4K8ac from protein extracts from whole sciatic DRGs after treatment with CSP or CSP-TTK21 for 5 weeks. Shown

is a significant increase in the expression of H4K8ac after treatment with CSP-TTK21 compared to CSP (mean  $\pm$  SEM, unpaired Student's t test, \*\*  $P < 0.01$ ,  $n = 3/\text{group}$ ). H4 was used to normalise the levels of H4K8ac and GAPDH was used as a loading control.

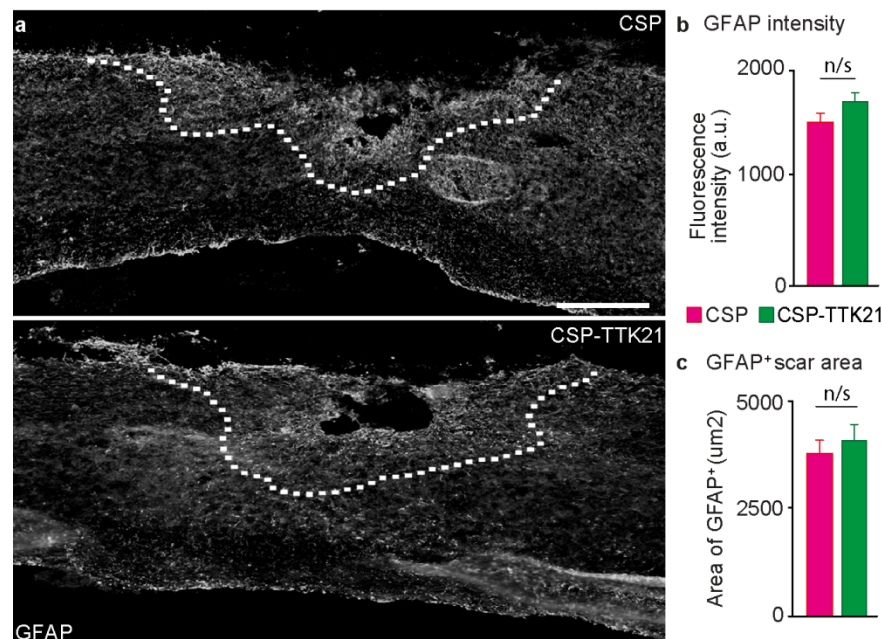


**Fig. S18. CSP-TTK21 treatment does not affect the glial scar after a thoracic dorsal spinal cord hemisection in mice.** (A) Example images of the T12 spinal lesion site immunolabelled for GFAP to identify reactive astrocytes and the glial scar after CSP or CSP-TTK21 treatment. Scale bar, 200  $\mu\text{m}$ . (B) Quantification of the area of GFAP positive scar showed no difference between CSP and CSP-TTK21 treated mice (mean  $\pm$  SEM, unpaired Student's t test,  $n = 8/\text{group}$ ). (C) Quantification of GFAP pixel intensity around the lesion site showed no difference between CSP and CSP-TTK21 treated mice (mean  $\pm$  SEM, unpaired Student's t test,  $n = 8/\text{group}$ ).

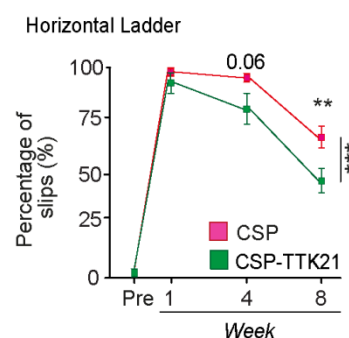


**Fig. S19. CSP-TTK21 significantly reduced the number of slips during locomotion along a horizontal ladder.** Quantification of percentage of slips (mean  $\pm$  SEM, Two-way repeated measures ANOVA, Sidak's post-hoc \*\*\* $P < 0.01$ , \*\* $P < 0.01$ ,  $n = 10/\text{group}$ ).

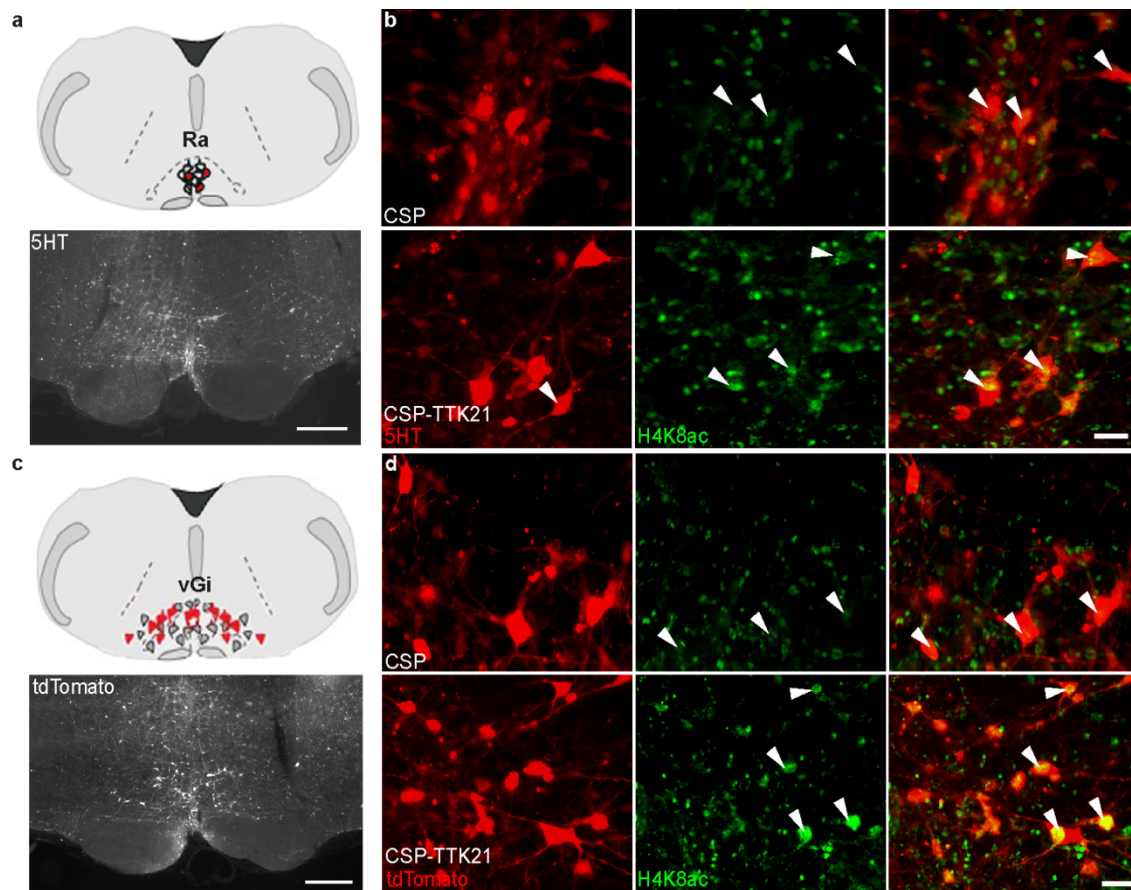


**Fig. S20. CSP-TTK21 treatment enhances levels of H4K8ac in the raphe nucleus and reticular formation.** (A) Schematic and representative image of the Raphe nucleus (Ra) stained for 5HT. (B) Treatment with CSP-TTK21 significantly enhanced H4K8ac (green) in 5HT positive neurons (red) in the Raphe nucleus. (C) Schematic and representative image of the ventral gigantocellular reticular nuclei (vGi) transduced with AAV8-CAG-DIO-tdTomato-COMET. (D) Treatment with CSP-TTK21 significantly enhanced levels of H4K8ac (green) in tdTomato positive neurons (red) in the vGi.

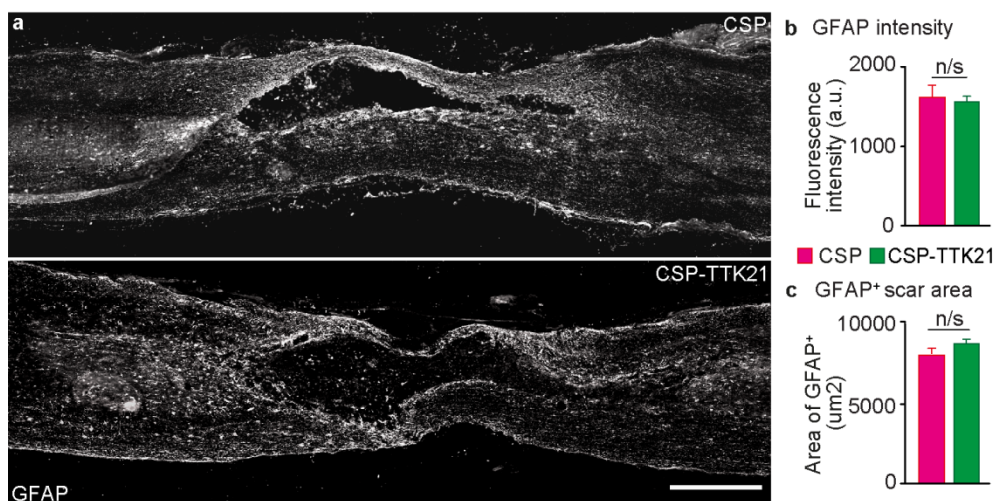


**Fig. S21. CSP-TTK21 treatment does not affect the glial scar after a thoracic contusion spinal cord injury in rats.** (A) Example images of the thoracic contusion site immunolabelled for GFAP to identify reactive astrocytes and the glial scar after CSP or CSP-TTK21 treatment. (B) Bar graph showing GFAP intensity (a.u.) for CSP and CSP-TTK21 groups. (C) Bar graph showing GFAP+ scar area (um<sup>2</sup>) for CSP and CSP-TTK21 groups.

Scale bar, 500  $\mu\text{m}$ . **(B)** Quantification of GFAP pixel intensity around the lesion site showed no difference between CSP and CSP-TTK21 treated mice (mean  $\pm$  SEM, unpaired Student's t test, n = 12/group). **(C)** Quantification of the GFAP positive scar area showed no difference between CSP and CSP-TTK21 treated rats (mean  $\pm$  SEM, unpaired Student's t test, n = 12/group).



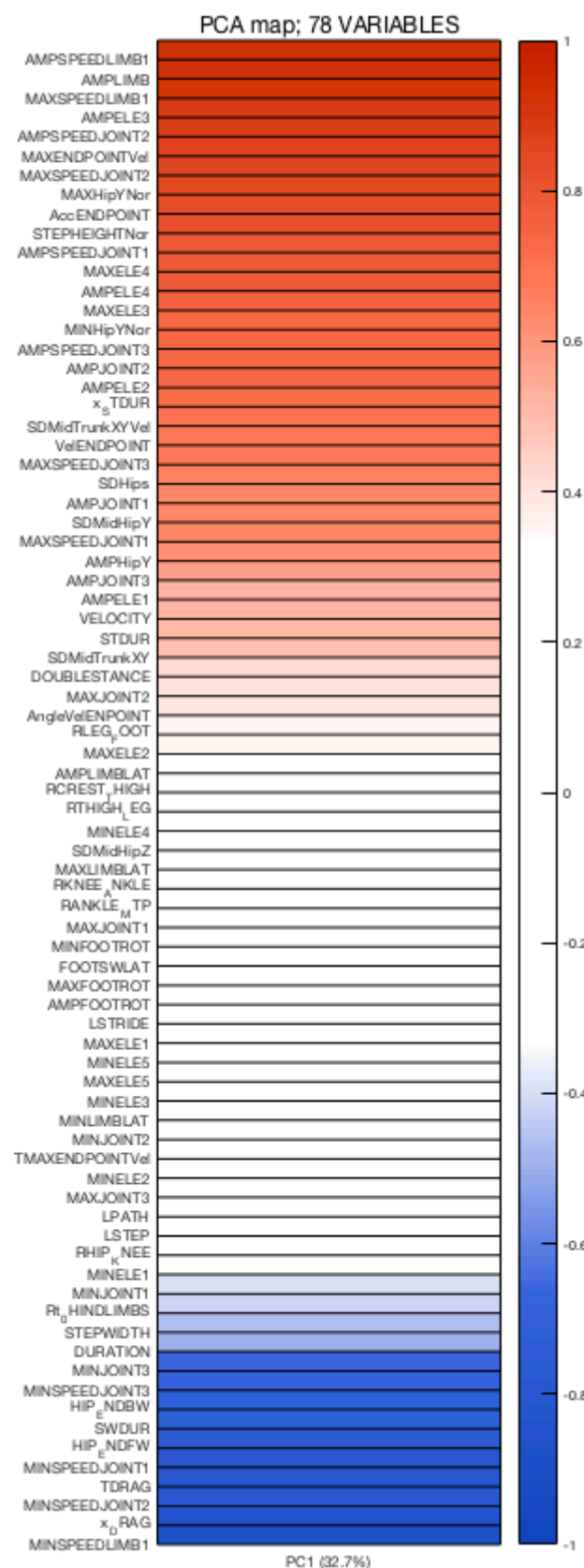


**Table S1.** Table compiling the 78 parameters used for quantifying gait features.



**Video S1. EE mediated calcium mobilization in proprioceptive DRG neurons.** Time-lapse video of intracellular calcium release from whole-mount PV-GCaMP DRGs. Mice were exposed to EE for 10 days before dissection and calcium imaging. A baseline recording was taken before the addition of 50 mM, 100 mM and 150 mM KCL. Videos are 20 fps.

**Video S2. SH mediated calcium mobilization in proprioceptive DRG neurons.** Time-lapse video of intracellular calcium release from whole-mount PV-GCaMP DRGs. Mice were exposed to SH for 10 days before dissection and calcium imaging. A baseline recording was taken before the addition of 50 mM, 100 mM and 150 mM KCL. Videos are 20 fps.

**Video S3. Treatment with CSP-TTK21 enhances hindlimb function and over-ground locomotion.** Example movies showing kinematic recordings of rats 8 weeks after a contusion SCI and treatment with CSP or CSP-TTK21.